Journal of Network and Computer Applications 51 (2015) 102–126

Contents lists available at ScienceDirect

Journal of Network and Computer Applications

journal homepage: www.elsevier.com/locate/jnca

Review

Modeling low-power wireless communications

Behnam Dezfouli [a,*], Marjan Radi [a], Shukor Abd Razak [a], Tan Hwee-Pink [b], Kamalrulnizam Abu Bakar [a]

[a] Department of Computer Science, Faculty of Computing, Universiti Teknologi Malaysia (UTM), Malaysia
[b] Networking Protocols Department, Institute for Infocomm Research (I^2R), Singapore

ARTICLE INFO

Article history:
Received 28 September 2013
Received in revised form
10 February 2014
Accepted 26 February 2014
Available online 12 March 2014

Keywords:
Simulation
Evaluation
Accuracy
Implementation

ABSTRACT

Low-power wireless communications have particular characteristics that highly affect the performance of network protocols. However, many of these essential characteristics have not been considered in the existing simulation platforms and analytical performance evaluation models. While this issue invalidates many of the reported evaluation results, it also impedes pre-deployment performance prediction and parameter adjustment. Accordingly, this paper studies, analyzes and proposes models for accurate modeling of low-power wireless communications. Our contributions are six-fold. First, we investigate the essential characteristics of low-power wireless transceivers. Second, we present a classified and detailed study on modeling signal propagation, noise floor, system variations and interference. Third, we highlight the importance and effects of system variations and radio regularity on the real applications of wireless sensor networks. Fourth, we reveal the inaccuracy of the packet reception algorithms used in the existing simulators. Furthermore, we propose an improved packet reception algorithm and we confirm its accuracy through comparison with empirical results. Fifth, we propose an architecture to integrate and implement the models presented in this paper. Finally, we show that the transitional region can be employed by the simulators to confine the propagation range and improve simulation scalability. To the best of our knowledge this is the first work that reveals the essentials of accurate modeling and evaluation of low-power wireless communications.

Contents

* Corresponding author.
E-mail address: dezfouli@ieee.org (B. Dezfouli).

http://dx.doi.org/10.1016/j.jnca.2014.02.009
1084-8045

1. Introduction

A low-power wireless network is a collection of nodes with scarce energy, computational and communication resources. As the radio transceiver is the major source of energy consumption, low-power wireless networks employ low-power wireless transceivers, which usually provide low data rate (tens of kbps), low transmission range (tens of meters) and poor link quality (Langendoen, 2008; Srinivasan et al., 2010; Chipcon CC2420, 2014; Chipcon CC1000, 2014).

Nowadays, low-power wireless networks such as wireless sensor networks are being used for various applications. Accordingly, the research community has paid significant attention to design protocols for these networks. However, as protocol development and evaluation through testbed is costly and time consuming, simulation is the widely used approach (Varshney and Bagrodia, 2004;Kuntz and Schmidt-Eisenlohr;Girod et al., 2007; Halkes and Langendoen, 2010). Meanwhile, due to the particular characteristics of low-power wireless communications (Srinivasan et al., 2010; Zhao and Govindan, 2003; Zamalloa and Krishnamachari, 2007), which highly affect the performance of network protocols, simulation reliability mainly depends on the accuracy of modeling wireless communications. Unfortunately, while significant study has been conducted on protocol design and improvement, considerably less attention has been paid to the importance of accurate performance evaluation. Therefore, when the simulation platform is not accurate, either the demonstrated performance cannot be expected in real-world scenarios, or the effects of wireless channel and transceiver on protocol performance are unclear.

1.1. State-of-the-art

The accuracy of modeling wireless communications mainly depends on the following issues: (i) *signal propagation and hardware modeling*; (ii) *inter-node interference modeling*; (iii) *external interference modeling*; (iv) *packet reception modeling*; (v) *propagation range*.

1.1.1. Signal propagation and hardware modeling

Motivated by the observations of Kotz et al. (2004), Ganesan et al. (2002), Halkes and Langendoen (2010), and Molina-Garcia-Pardo et al. (2005), which invalidate the existence of a fixed and circular transmission range for all the nodes, various models have been proposed for multipath effect, radio irregularity, hardware heterogeneity and bit error rate. In particular, the studies reported in Zamalloa and Krishnamachari (2004, 2007) confirmed the accuracy of the log-normal shadowing model to represent the link variations caused by multipath channel. In addition, these works investigate hardware heterogeneity in terms of transmission power and noise floor differences for similar nodes. The results presented in Ganesan et al. (2002) and He et al. (2003) showed the existence of radio irregularity around low-power transmitters. This property reveals the significant variations of received signal power versus direction changes around a transmitter. Accordingly, the radio irregularity model (RIM) has been proposed in Zhou et al. (2006) to represent this behavior. With respect to the transceiver modulation types, various models have been proposed to map SINR to bit error and packet error probability (Rappaport, 2002; IEEE Computer Society, 2012; TOSSIM, 2014).

1.1.2. Inter-node interference modeling

Since the wireless channel is a broadcast medium, and with respect to multihop communications, interference modeling is particularly important as it defines how a signal reception would be affected by the interfering signals caused by other nodes

(Cardieri, 2010; Son et al., 2006; Zhang et al., 2007; Lee et al., 2010a). To this aim, various interference models with different accuracy and complexity have been proposed. Accordingly, studies such as Iyer et al. (2009), Maheshwari et al. (2008a), Maheshwari et al. (2008b), Halkes and Langendoen (2010), Cardieri (2010), and Lee et al. (2010a) tried to analyze these models. These studies, in particular, reveal that considering additive interference through the SINR model is essential for accurate performance evaluation.

1.1.3. External interference modeling

When the frequency band of the communicating nodes is affected by other networks or devices, external interference modeling is valuable to reflect network performance in real environments. To this aim, few studies have been conducted to model external interference at 2.4 GHz band (Srinivasan et al., 2010; Lee et al., 2007c).

1.1.4. Packet reception modeling

This specifies how a packet reception algorithm employs an interference model during packet reception. Therefore, interference modeling highly affects the accuracy of packet reception modeling. For example, in NS2 CTM[1](NS-2, 2014) the interference model is only used at packet arrival (Ryu et al., 2008). In contrast, the SINR model can be used in various ways to achieve different accuracy levels in packet reception modeling. For example, in NS2 SINR (NS-2, 2014), the SINR model is used at each packet arrival and after a successful preamble reception (Chen et al., 2007). Unfortunately, even the packet reception algorithm of NS3 (NS-3, 2014) presents inaccuracies in the performance evaluation of low-power networks. Although some studies have revealed the inaccuracy of these models in specific scenarios (Papanastasiou et al., 2010; Hamida et al., 2008; Al-Bado et al., 2012; Lee et al., 2010a), their implications on the performance evaluation of low-power wireless networks have not been investigated. Furthermore, no improvement has been proposed for these models.

1.1.5. Propagation range

Propagation range specifies the maximum range at which a node's transmission should affect other nodes. Therefore, as longer propagation range causes lower simulation speed, propagation range confinement is essential for providing simulation scalability. With respect to the additive property of interference, several studies showed that inaccurate confinement of propagation range considerably reduces the simulation accuracy (Hamida et al., 2008; Hu and Hou, 2005). The existing propagation range confinement methods are either complicated and cannot be used in various network configurations, or they are very simple and cause inaccurate evaluation results.

1.2. Motivations and contributions

(i) Low-power wireless networks employ specific transceivers with unique characteristics. As the first contribution of this paper we study the characteristics and design implications of the commonly used low-power transceivers.

(ii) To the best of our knowledge, despite the existence of diverse models, there exists no study to investigate and categorize the existing models proposed for low-power wireless communications. The second contribution of this paper is to present a classified and detailed study of these models. While this study helps to highlight the inaccuracies of the existing simulation tools, it also enables the researchers to be aware of the essential models that should be considered in the developed simulation tools and analytical performance evaluations.

(iii) A body of protocols can be found in the literature that aim to improve the performance of low-power networks. Unfortunately, since the effects of the essential characteristics of low-power wireless communications on the performance of network protocols are not clear, these characteristics are usually neglected by simulation tools. Accordingly, as the third contribution of this paper we evaluate the effects of system variations and radio irregularity on the realistic applications of wireless sensor networks. We show that, while most of the network simulators do not model these characteristics, considering these effects is essential for accurate performance evaluation.

(iv) Although recent studies on interference models have confirmed the accuracy of the SINR model, the relationship and potential effects of interference modeling and packet reception algorithms are still unclear. As the fourth contribution of this paper we investigate and highlight the impreciseness of the packet reception algorithms used in network simulators. First we identify the shortcomings of employing the capture threshold model in the network simulators such as NS2 CTM. Then, we show that, although employing the SINR interference model by packet reception algorithms improves packet capture accuracy, network simulators such as NS2 SINR suffer from considerable error in evaluating low-power networks. To address these shortcomings, we propose an improved packet reception algorithm that provides higher accuracy compared with the existing algorithms. The inaccuracy of the NS2 packet reception algorithms and the significantly higher accuracy of the proposed algorithm are demonstrated through comparison with empirical results.

(v) Since none of the existing simulation tools implement all the essential models required for evaluating low-power networks, the fifth contribution of this paper is to propose an architecture within which these models can be implemented. This architecture along with the proposed packet reception algorithm is used to develop an accurate simulation tool on the OMNeT++ simulation framework. We also discuss about the effect of each model on simulation speed.

(vi) As the sixth contribution of this paper, we study the existing approaches used by the simulation tools to improve simulation speed through reducing the overhead of signal propagation. Using the developed simulation tool, we change the radio propagation range and measure its effects on performance evaluation. Through comparison with the existing models, we show that the transitional region size provides a straightforward way to confine the propagation range.

1.3. Paper organization

In Section 2, we study the important characteristics of low-power transceivers. Section 3 presents the models required for accurate performance evaluation. We describe the methodology employed for performance evaluations in Section 4. Section 5 presents the analyses that reflect the importance and effects of modeling system variations and radio irregularity. In Section 6, we carefully analyze the packet reception algorithms used by NS2. We also propose an improved packet reception algorithm. In Section 7, we present an architecture to integrate and implement the essential models of simulating wireless networks. Additionally, we evaluate the effects of propagation range. Table 1 summarizes the key notations used in this paper.

2. Low-power RF transceivers

In this section, we study the characteristics of low-power wireless transceivers. Table 2 presents the main features of five transceivers. Since CC1000 and CC2420 are the radios employed by

[1] In this paper we refer to NS2.32 and its predecessors as NS2 CTM, and NS2.33 and its successors are referred to as NS2 SINR.

Table 1
A summary of key notations.

Description	Symbol
A signal transmitted by node i	S_i
The set of the signals currently being received at a node	$\mathbf{S}$
Output power of node i	Ω_i
Output power of node i considering hardware heterogeneity	Ω_i^{adj}
Received power at node j, corresponding to signal S_i	$\Psi_j(S_i)$
Average noise floor	$\overline{\Psi}$
Noise floor of node i considering hardware heterogeneity	$\overline{\Psi}_i^{adj}$
MAC protocol data unit (MAC header+payload+CRC)	MPDU
Number of required bits for signal synchronization	$L_{settling}$
Number of MPDU bits	L_{MPDU}
Total number of bits in a packet	L_{packet}
SINR value corresponding to signal S_i	$SINR(S_i)$
SINR value at node j, corresponding to signal S_i, at time t	$SINR_j(S_i, t)$
The set of nodes in the network	$\mathbf{V}$
Radio speed	R
Path-loss exponent	η
Standard deviation of multipath channel variations	σ_{ch}
Standard deviation of additive white Gaussian noise	σ_{WGN}
Standard deviation of transmission power heterogeneity	σ_{tx}
Standard deviation of noise floor heterogeneity	σ_{rx}

the commonly used wireless sensor nodes (such as Mica2, 2014; MicaZ, 2014; TelosB, 2014), we provide additional explanations regarding these transceivers.

2.1. Signal synchronization

In low-power wireless communications, regardless of the utilized transceiver module, receiver should obtain certain information about the incoming signal before receiving data. To this aim, data packets begin with a predefined training sequence, called *preamble*, which enables the receiver to learn about the parameters of the transmitter. In addition to the preamble bytes, the receiver should be able to detect the start and the end of the data frame. Therefore, specific bytes should be transmitted immediately after the preamble bytes. These bytes are called *sync word* or *start of frame delimiter (SFD)*. The total duration of the preamble and sync bytes is usually referred to as the *physical-layer header*. To achieve accurate synchronization, each radio defines a minimum number of bits that should be received before actual data reception. In this paper, the minimum number of synchronization bits located at the end of the preamble is referred to as the *settling bits*.

CC1000: As this is a byte-base radio (cf. Section 2.2), the size and pattern of the preamble bits can be configured by the user. However, the minimum preamble size depends on the configured acquisition mode and receiver sensitivity. For example, to achieve the highest sensitivity level in Manchester mode, preamble duration should be at least 98 bits long. To satisfy this requirement, the implementation of B-MAC (Polastre et al., 2004) in TinyOS (2013) uses 10 bytes as the physical-layer header.

CC2420: The default preamble size is 4 bytes, which provides compatibility with the IEEE 802.15.4 standard (IEEE Computer Society, 2012). In addition, it is recommended to avoid using preambles shorter than 4 bytes, because it may increase the number of false packet detections.

Although using the minimum required preamble size reduces the overhead of packet transmission, low-power MAC protocols usually employ the low-power listening mechanism (LPL) (Polastre et al., 2004; Jurdak et al., 2007), which requires using large preambles. For example, while the required number of settling bits for CC1000 radio is about 6 bytes, B-MAC with 200 ms sampling interval uses 480-byte preambles. In this case, even if a signal's SINR value is not strong enough during the first 474 bytes of the preamble, providing enough SINR value during

Table 2
Low-power RF transceivers and their characteristics

Transceiver	**TR1000** (TR1000, 2014)	**CC1000** (Chipcon CC1000, 2014)	**CC1120** (CC1120, 2014)	**CC2420** (Chipcon CC2420, 2014)	**CC2500** (CC2500, 2014)
Radio type	Narrowband	Narrowband	Narrowband	Wideband	Wideband
Byte/packet oriented	Byte oriented	Byte oriented	Packet oriented	Packet oriented	Packet oriented
Operating frequency	916/868 MHz	315/433/868/ 916 MHz	170/315/433/ 868/915/920/ 950 MHz	2.4 GHz	2.4 GHz
Max data rate [kbps]	115.2	76.8	200	250	500
Modulation	OOK/ASK	FSK	2-FSK/2-GFSK/ 4-FSK/4-GFSK/ MSK/ OOK	DSSS-O-QPSK	OOK/2-FSK/ GFSK/MSK
Output power [dBm]	1.5	−20 to 10	−40 to 16	−24 to 0	−30 to 0
TX power [mA]	12 (1.5 dBm)	10.4 (0 dBm, 433 MHz) 16.5 (0 dBm, 868 MHz)	26 (0 dBm, 950 MHz)	17.4 (0 dBm) 8.5 (−25 dBm)	21.2 (0 dBm) 11.1 (−12 dBm)
RX power [mA]	3 (2.4 kbps) 3.8 (115.2 kbps)	7.4 (433 MHz) 9.6 (868 MHz)	22	19.7	12.8 (2.4kbps) 19.6 (500kbps)
Sleep power [μA]	0.7	0.2–1	0.3–1	1	0.4
Startup time [ms]	0.016	2	0.4	0.86, 0.3 (power ramp-up time)	0.3, 5 (power ramp-up time)
Receiver sensitivity (Best) [dBm]	−106 (2.4 kbps, ASK)	−110 (1.2 kbps, 433 MHz)	−127 (300 bps) −103 (200 kps)	−94, −85 for 802.15.4	−104 (2.4 kbps, FSK)

the last 6 bytes of the preamble can result in successful synchronization. We will later show that employing long preambles requires specific design considerations regarding packet reception modeling (cf. Section 6).

2.2. Packet formatting

Based on the packet formatting mechanism, the existing low-power RF transceivers can be categorized into two groups: *byte-oriented* and *packet-oriented*. A byte-oriented radio (e.g., CC1000) does not provide any packet formatting mechanism by the radio's hardware. Hence, in addition to the data bytes, microcontroller should generate and transmit the preamble, sync word and CRC bits into the radio module. As the radio merely transmits the data received from the microcontroller, every transmitted bit can be controlled by the user. Therefore, by using byte-oriented radios, protocol designers can easily define their own packet format, based on the requirements of upper-layer protocols. The hardware of packet-oriented radios (e.g., CC2420) defines a specific packet format that usually follows a specific standard (e.g., 802.15.4). Although these radios allow new packet format definition, the provided flexibility is less than that provided by byte-oriented radios. For example, as packet-based radios define a maximum packet length imposed by their transmission buffer, it may be infeasible to achieve a desired preamble duration, which is required for LPL-based MAC protocols. In this case, multiple packets can be transmitted to act as a long preamble and wake up the receiver (Ye et al., 2006). On the other hand, new radios (such as CC2500) provide some features to support the LPL mechanism.

CC1000: This radio does not provide any data buffer. Therefore, despite its packet formatting flexibility, finding the SFD bytes to identify actual data bytes should be implemented by software.

CC2420: Although it supports the 802.15.4-compliant packet format, it also allows for packet formatting. However, as this transceiver provides two separate 128-byte memory banks for packet transmission and reception, it does not support packet sizes larger than 127 bytes (one byte is reserved for packet size).

2.3. Modulation types

Wireless transceivers can be categorized based on their modulation type: *narrowband* and *wideband*. While narrowband radios can achieve longer transmission range with lower energy consumption, wideband radios spend more energy, because they spread the signal over a wider range to provide higher interference immunity. Additionally, since wideband radios provide higher data rate, they operate at 2.4 GHz due to the larger available bandwidth.

CC1000: This transceiver can be configured to operate at frequency range 300–1000 MHz, with different transmission and reception frequencies. The very fast frequency shifting capability of this radio makes it suitable for implementing frequency hopping protocols.

CC2420: In compliance with the 802.15.4 standard, CC2420 can be programmed to operate at 16 different channels, numbered from 11 to 26. Therefore, its multichannel capability can be utilized by the MAC protocols to increase network throughput. Although CC2420 uses the Direct Sequence Spread Spectrum (DSSS) modulation, studies showed that most of the channels suffer from significant interference from other 2.4 GHz transmitters (Lee et al., 2007c; Rusak and Levis, 2008) (cf. Section 3.8).

2.4. The capture effect

As low-power radios utilize omnidirectional antennas, and due to the broadcast nature of the wireless channel, inter-node interference highly affects packet reception performance, which reflects in network throughput capacity (Son et al., 2006; Maheshwari et al., 2008a; Woo and Kim, 2010; Iyer et al., 2009). Meanwhile, the capture effect (a.k.a., co-channel interference tolerance (Kim and Lee, 1999)) is a characteristic of wireless transceivers that allows the reception of the stronger signal at the presence of weaker signal sources. With this definition, a packet arrival during an ongoing packet reception may not corrupt both of the packets if one of the packet's SINR is higher than a certain threshold. Figure 1 shows sample scenarios in which the stronger signal is the firstly (Fig. 1(a)) and secondly arrived signal (Fig. 1(b)).

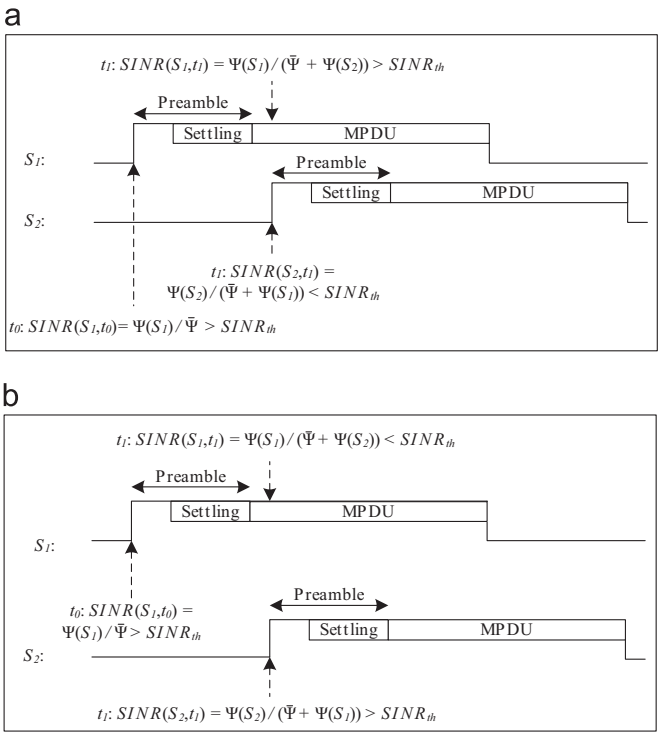

Fig. 1. (a) Strongest-first packet capture: packet S_1 can be completely received, because its SINR is higher than the threshold value even after the arrival of S_2. (b) Stronger-last packet capture: although the radio is receiving packet S_1 during t_0 to t_1, it switches to receive S_2 at time t_1, because the SINR of this signal is higher than S_1, and it is higher than the threshold value.

The importance of accurate modeling of the capture effect in network simulation can be justified through two main reasons: (i) As the capture effect is supported by most of the wireless transceivers (Son et al., 2006; Lu and Whitehouse, 2009; Lee et al., 2007a; Whitehouse et al., 2005), this feature significantly affects packet reception performance when packets are subject to interference. More specifically, studies on the capture effect in low-power (Son et al., 2006; Whitehouse et al., 2005; Gezer et al., 2010; Firner et al., 2010) and IEEE 802.11 wireless networks (Lee et al., 2007a; Kochut et al., 2004) have revealed that the capture effect increases packet reception probability when multiple packets collide at a receiver, and the capture effect causes packet reception unfairness. (ii) The capture effect can be used for protocol optimization. For example, it has been used for collision detection (Yun and Seo, 2007; Whitehouse et al., 2005; Dezfouli et al., 2014), packet loss reduction (Firner et al., 2010), flood propagation enhancement (Lu and Whitehouse, 2009), and packet reception improvement through interference management (Xu et al., 2010).

3. Modeling low-power wireless communications

The aim of this section is to present the essential characteristics of low-power wireless communications, as well as the models

proposed for these characteristics. Accordingly, we study the existing models proposed for radio propagation, bit error computation and interference.

3.1. Signal propagation

A signal sent by a wireless transmitter loses its power as it moves away from the sender. The three well-known models of signal decay are (Rappaport, 2002): (i) *free-space propagation model*, (ii) *ground reflection (two-ray) model*, and (ii) *log-normal shadowing model* (which is an elaboration over the *log-distance path-loss model*).

Although the ground reflection model includes the effects of ground reflection path and provides higher accuracy than the free-space propagation model, both of these models represent signal strength as a fixed function of distance. This representation results in a circular communication range, which is referred to as the *unit disk graph model* (UDG). However, experimental evaluation of low-power links indicates the existence of three distinct regions around a sender (Zamalloa and Krishnamachari, 2007; Woo et al., 2003; Zhao and Govindan, 2003; Reijers et al., 2004): *connected* (packet reception ratio is higher than 90%), *transitional* (packet reception ratio varies between 90% to 10%), and *disconnected* (packet reception ratio is lower than 10%). Therefore, the UDG model has been criticized by the researchers, because the theoretical and simulation-based performance evaluation of the protocols designed with this assumption are different from the expected real-world results (Seada et al., 2004; Ganesan et al., 2002; Reijers et al., 2004; Kotz et al., 2004). In contrast to the free-space and ground reflection models, the log-normal shadowing model includes the effects of multipath propagation and represents signal strength at a given distance as a random variable. Specifically, Nikookar and Hashemi (1993) showed that the log-normal distribution provides a more accurate multipath fading model than the Rayleigh and Nakagami distributions. The log-normal shadowing model is

$$PL(d) = PL(d_0) + 10\eta \log_{10}\left(\frac{d}{d_0}\right) + N(0, \sigma_{ch}) \quad (1)$$

where d is the distance from the sender, $PL(d)$ is the path loss at distance d, d_0 is the reference distance (a.k.a., *close-in distance*), $PL(d_0)$ is the path loss at the reference distance, η is the path-loss exponent, $N(0, \sigma_{ch})$ is a zero-mean Gaussian random variable with standard deviation σ_{ch}, and σ_{ch} is the variations of signal power due to the multipath channel. It has been shown that this equation holds for both indoor and outdoor environments (Rappaport, 2002; Zamalloa and Krishnamachari, 2004).

Sohrabi et al. (1999) conducted extensive experiments to determine channel parameters for the log-normal shadowing model in the frequency range 800–1000 MHz for different environments. Their results indicate path-loss exponent from $\eta = 1.9$ (for a multi-leveled engineering building) to $\eta = 5$ (for a bamboo jungle). They also showed 30–50 dB loss in signal power at the reference distance 1 m. Similar experiments have also been conducted by Zamalloa and Krishnamachari (2004, 2007) to obtain the channel parameters using CC1000 radio in indoor and outdoor environments. Although the general validity of the log-normal shadowing model has been confirmed for various transceivers (Chen and Terzis, 2011; Son et al., 2007; Zamalloa and Krishnamachari, 2007), specific parameters should be used for each radio. For example, in a given environment, the log-normal shadowing model requires different parameters for CC1000 and CC2420 transceivers, which is due to the differences in the frequency and modulation types used in these transceivers. Table 3 summarizes the parameters of the log-normal shadowing model for CC1000 and CC2420 radios.

Using Eq. (1), Fig. 2 shows how path-loss exponent and multipath variations affect the size of the connected and transitional regions. The main observations from this figure are: Firstly, for a given multipath value, reducing the path-loss exponent results in significantly higher increase in the transitional region size, compared with the connected region size. Therefore, as Table 3 indicates lower path-loss exponent for the CC2420 radio, this radio causes larger transitional region and more number of links with poor quality. Secondly, for a given path-loss exponent, increasing the multipath variations results in lower size of the connected region and larger size of the transitional region. Section 5.1 provides further studies regarding the effects of system variations on the performance of wireless sensor networks.

The importance of employing an accurate signal propagation model is intuitive. For example, the effects of the constant and variable part of the log-normal shadowing model can be discussed

Table 3
The parameters of the log-normal shadowing model for CC1000 and CC2420 radios and for different environments (Chen and Terzis, 2011; Zamalloa and Krishnamachari, 2007; TOSSIM, 2014; Evans et al., 2012; Shin et al., 2005; IEEE Computer Society, 2003).

		Environment				
		Indoor		Outdoor		
	$PL(1)$	52.1		55.4		
CC1000	η	3.3 (2.1–4.5)		4.7 (4.3–5.1)		
	σ_{ch}	5.5 (4.6–6.8)		3.2 (2.6–3.8)		
		Hallway	Office	Parking	Lawn	Forrest
CC2420	$PL(2)$	53.9	49.9	59.2	56.4	57.4
	η	1.82	1.97	3	3.6	2.08
	σ_{ch}	5.5 (4.6–6.8)		3.2 (2.6–3.8)		

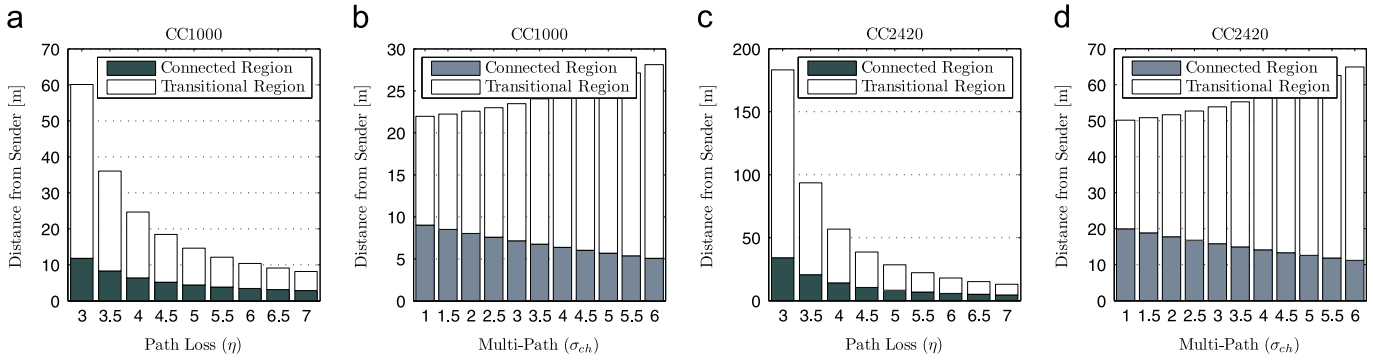

Fig. 2. Effects of path-loss exponent and multipath variations on the extent of the connected and transitional region for CC1000 and CC2420 transceivers. In figure (a) and (c) the multipath value is 4. In figure (b) and (d) the path-loss exponent is 4.

as follows. First, the fixed part (i.e., $PL(d_0)+10\eta \log_{10}(d/d_0)$) highly affects signal relationship between nodes. As signal relationship between nodes determines network capacity, accurate path-loss modeling is crucial. Second, the variable part (i.e., $N(0,\sigma_{ch})$) models signal variations, which also affects signal relationship between nodes. More specifically, as this part contributes to SINR variations during packet reception, it affects packet reception performance. Both parts of the log-normal shadowing model influence higher-layer protocols such as MAC and routing. For example, higher multipath variations increase the number of hops to the sink node, as Fig. 2 and Section 5.1 show. Additionally, for example, signal variations affect carrier-sensing performance.

The log-normal shadowing model has widely been utilized in the low-power wireless networking literature for mathematical analysis, protocol design, protocol evaluation, etc. Ji et al. (2004), Martnez-Sala and Molina-Garca-Pardo (2005), Seada et al. (2004), Kuntz and Schmidt-Eisenlohr, Chen and Terzis (2011), and Seidel and Rappaport (1992). Furthermore, this model has been used in many of the wireless network simulators.

3.2. Noise floor

Noise floor of a transceiver affects its reception sensitivity and it is mainly caused due to two reasons: hardware noise and environmental noise. As stated in Rappaport (2002), the *noise figure* of a transceiver provides a convenient way to compute its noise floor,

$$\overline{\Psi} = (F+1)\cdot k\cdot T\cdot B \tag{2}$$

where $\overline{\Psi}$ is the noise floor, F is the transceiver's noise figure (not in dB), k is the Boltzmann's constant, T is the environmental temperature, and B is the system noise bandwidth. Assuming the environmental temperature is 300 °K, Table 4 shows the noise parameters and noise floor values for CC1000 and CC2420. As it can be observed, the real noise floor (empirically measured) values are higher than the computed values. This is caused by the circuit between the antenna and chip, and environmental noise (Zamalloa and Krishnamachari, 2004; Srinivasan et al., 2010).

While Eq. (2) presents the noise floor as a fixed value, empirical evaluations have confirmed noise floor variability (Ganesan et al., 2002; Son et al., 2006; Zamalloa and Krishnamachari, 2007; Karl and Willig, 2005; Polastre et al., 2004). Specifically, it has been pointed out that in addition to the spatial link variations modeled by Eq. (1), signal variations against time are mainly caused by noise fluctuations. Therefore, the variations of noise floor versus time caused by the white Gaussian noise can be represented as

$$\overline{\Psi}(t) = N(\overline{\Psi}, \sigma_{WGN}) \tag{3}$$

where $\overline{\Psi}(t)$ is the noise floor at time t, and σ_{WGN} is the standard deviation of white Gaussian noise. Unfortunately, the literature does not report consistent values for representing noise floor variations. For example, Son et al. (2006) and Srinivasan et al. (2010) report small variations in noise floor (<1 dB). However, the noise floor variability considered in TOSSIM (2014) is about 4–5 dB, which is very similar to the measurements conducted by Polastre et al. (2004). Analysis of noise floor variations in various environments and for different transceivers would be a potential area of future work.

It is worth mentioning that the method described in this section is used to model noise floor in the absence of external interference. Therefore, accurate noise modeling may also require employing an external interference model (cf. Section 3.8). This is particularly important when the 2.4 GHz band is in use (e.g., with CC2420), since this band is shared by many devices.

As noise floor defines receiver sensitivity, it affects interference immunity. For example, if node i is able to receive from node j when a collision occurs due to the transmission of node k, increasing the noise floor of node i reduces the SINR value of signal j and may affect packet reception from node j. Furthermore, noise floor variations cause changes in the SINR of the signals being received. Noise floor also affects carrier-sensing performance, which appears in the efficiency of collision avoidance mechanisms. For example, a node with lower noise floor could sense farther transmissions and provide higher collision avoidance capability.

3.3. Bit error probability

Bit error probability (a.k.a., bit error rate (BER)) refers to the probability of an incorrect bit reception. Usually, for a given modulation scheme, bit error rate is represented as a function of E_b/N_0, where it refers to the energy per bit (E_b) to the spectral noise density (N_0) (Rappaport, 2002). For example, for the NCFSK modulation used in CC1000 radio, bit error rate is given as

$$\Pr(\overline{\text{bit}})_{NCFSK} = \frac{1}{2}\exp^{-E_b/(2N_0)} \tag{4}$$

where $\Pr(\overline{\text{bit}})$ is the probability of bit error. Since $E_b/N_0 = SINR\times B/R$, Eq. (4) can be used to determine bit error rate against SINR (not in dB). Here, B is the noise bandwidth and R is the radio bit rate.

For CC2420 radio, which employs the 16-OQPSK modulation, BER can be computed from SINR (not in dB) as (IEEE Computer Society, 2012),

$$\Pr(\overline{\text{bit}})_{16-OQPSK} = \frac{8}{15}\times\frac{1}{16}\times\sum_{k=2}^{16}(-1^k)\binom{16}{k}e^{20\cdot SINR\cdot(\frac{1}{k}-1)} \tag{5}$$

Various transceivers employ different modulation schemes and represent different SINR requirements for packet reception. Reducing the SINR value required for correct packet reception results in higher interference immunity and increases network capacity. In addition, for example, through considering the SINR value required for packet reception, a TDMA MAC protocol could employ tighter schedules for performance improvement.

3.4. Packet reception probability

While bit error rate depends on the environmental and transceiver characteristics, packet reception probability (a.k.a., packet reception ratio (PRR)) also depends on the encoding scheme (e.g., NRZ, Manchester, SECDEC). For example, for Manchester encoding (which is supported by the CC1000 hardware), 1 baud = 0.5 bit, therefore,

$$\Pr(\text{packet}) = (1-\Pr(\overline{\text{bit}}))^{2\cdot L_{packet}} \tag{6}$$

where $\Pr(\text{packet})$ is the probability of correct packet reception and L_{packet} is the packet size.

Table 4
The noise parameters, theoretical noise floor and empirical noise floor of CC1000 and CC2420 transceivers (Srinivasan et al., 2010; Zamalloa and Krishnamachari, 2007; Son et al., 2006).

Transceiver	Noise figure (F) [dB]	Noise bandwidth (B) [KHz]	Computed noise floor [dBm]	Real noise floor [dBm]
CC1000	12/13	30	−115/−116	−105/−106
CC2420	15.3	194	−105	−98

Eq. (6) shows packet reception probability as a function of total packet size; however, successful reception of all the preamble bytes is not required for successful packet reception. In particular, as low-power wireless networks usually employ long preambles to implement the LPL technique, a packet may be received without complete reception of its preamble bytes. With respect to the definitions given in Section 2.1, the probability of correct packet reception can be given as

$$\Pr(\text{packet}) = (\Pr(\text{bit})_{settling})^{L_{settling}} \times (\Pr(\text{bit})_{MPDU})^{L_{MPDU}} \quad (7)$$

where $\Pr(\text{bit})_{settling}$ is computed through considering the SINR value during the settling bits, and $\Pr(bit)_{MPDU}$ is computed through considering the SINR value during the MPDU.

Computing bit error rate to decide about correct packet reception has been used in simulators such as GloMoSim (2014), Castalia (2011), NS-3 (2014) and MiXiM (2014). After computing Pr(packet) it is compared with a random number in range [0,1] to determine packet reception status. Unfortunately, these simulators do not account for packet synchronization. In other words, successful packet reception depends on the correct reception of all the preamble bytes. Therefore, these simulators do not provide an accurate estimation of packet reception performance. NS2 CTM and NS2 SINR do not compute bit error rate. Rather, a packet is received if its SINR is higher than a specific threshold value. The threshold value is set based on empirical observations. In TOSSIM (2014), instead of computing bit error rate based on transceiver specifications, an empirical trace is used to determine packet reception ratio. Specifically, TOSSIM employs the following function for SINR to PRR mapping,

$$\Pr(\text{packet}) = \left(1 - \frac{1}{2}\text{erfc}(a_1 \times \sqrt{\frac{|SINR - a_2|}{2}})\right)^{2\times 23} \quad (8)$$

where erfc is the complementary error function, $a_1 = 1.3687$ and $a_2 = 0.9187$. Unfortunately, this function only fits the empirical results of using 23-byte packet, and cannot be used for other packet sizes.

Although this section provided a general overview of packet reception modeling, Section 6 presents further details regarding the existing packet reception algorithms.

3.5. Anisotropic path loss

According to the log-normal shadowing model, signal variations at distance d are mainly caused by the multipath effect, which can be modeled through a Gaussian random variable. Ganesan et al. (2002) conducted various experiments to measure packet reception ratio at different directions around the nodes with TR1000 transceiver. Their results revealed that, except signal variations at a given direction, radio propagation is not isotropic and demonstrates significant variations against direction changes. For example, assuming that a receiver is at the north direction of a sender, changing the direction of the receiver reveals significant changes in the average packet reception ratio. They called this phenomenon *directionality*. The importance and characteristics of radio irregularity have also been studied by Stankovic et al. (2005), Lee et al. (2010b), Biaz (2005), Ababneh (2009), and Muetze et al. (2008). Zhou et al. (2006) carried out experimental evaluations with CC1000 and CC2420 transceivers, and confirmed the previous observations through introducing the existence of *radio irregularity*. In order to justify this phenomenon, they presented two main reasons causing anisotropic path loss: (i) Since a propagated signal may be reflected, diffracted and scattered (Rappaport, 2002), and due to the environmental differences, signal path loss varies at different directions. (ii) The antenna gain may not be the same at different directions. Interestingly, their results showed that CC2420 exhibits higher irregularity in the radio pattern, compared with CC1000.

Zhou et al. (2006) characterized radio irregularity as follows: (i) *Anisotropy*: a signal transmitted by a node experiences various path losses at different directions; (ii) *Continuous variations*: path-loss variations around a sender is continuous with respect to the directional changes. In order to model these behaviors, they elaborated the *DOI* (degree of irregularity) model of He et al. (2003), and defined it as the maximum percentage of variations in path loss versus the changes in the propagation direction (denoted in unit degree). Accordingly, they proposed the *radio irregularity model* (RIM), which can represent the anisotropy and continuous variations of path loss. This path-loss model is given as follows:

$$PL(d,\theta) = \left(PL(d_0) + 10\eta \log_{10}\left(\frac{d}{d_0}\right)\right) \cdot K_\theta + N(0,\sigma_{ch}) \quad (9)$$

where $PL(d,\theta)$ is the DOI-adjusted path loss at direction θ, and K_θ is the path-loss coefficient at direction θ. K_θ is computed as

$$\begin{cases} \text{if } \theta = 0 : K_\theta = 1 \\ \text{if } 0 < \theta < 360 : \begin{cases} \text{if } B(1,0.5) = 0 : \\ \quad K_\theta = K_{\theta-1} + W(b_1,b_2) \times DOI \\ \text{if } B(1,0.5) = 1 : \\ \quad K_\theta = K_{\theta-1} - W(b_1,b_2) \times DOI \end{cases} \end{cases} \quad (10)$$

where $0 < \theta < 360$ and $\theta \in \mathbb{N}$, $|K_0 - K_{359}| < DOI$, $B(n,p)$ is a Binomial random variable with n trials and success probability p, and $W(b_1,b_2)$ is a Weibull random variable with scale parameter b_1 and shape parameter b_2. To characterize the Weibull distribution,

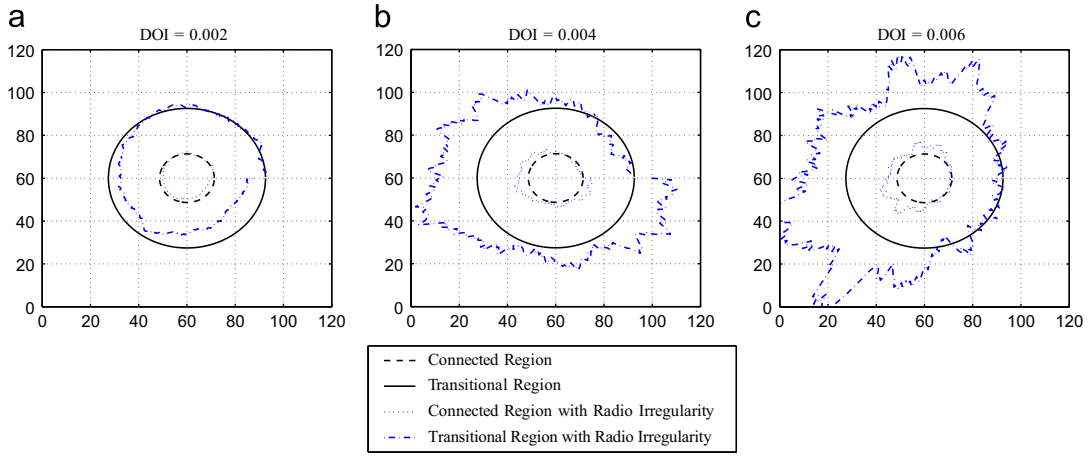

Fig. 3. Effect of radio irregularity on the size and shape of the connected and transitional regions. The *x*- and *y*- axes show the distance in meter.

Zhou et al. have reported various parameter sets that could fit their experimental results. For non-integer θ values, K_θ can be obtained through the interpolation of the two adjacent values.

In order to further clarify the effects of radio irregularity, in Fig. 3 we show the connected and transitional regions for various DOI values. This figure specifically indicates the insufficiency of the log-normal shadowing model for simulating link connectivity and unreliability.

Zhou et al. performed various experiments with Mica2 and MicaZ nodes to measure their DOI value. Since each node has its own DOI value, and it is not feasible to enter a unique DOI value for each node in a measurement study, they proposed to use the *VDOI* parameter, which reflects the variance of DOI. Using the Gaussian distribution, each node can choose its DOI value through $N(DOI, VDOI)$. Their study also shows that the accuracy of the RIM model can be improved through increasing the number of simulated nodes. For example, for a given DOI value, they observed that increasing the number of nodes from 100 to 1000 reduces the ratio of the confidence interval to the input value from 2.7% to 0.8%.

Except the inherent causes of path-loss anisotropy, obstacles also affect path-loss intensity. Assuming an obstacle position is known, Zamalloa and Krishnamachari (2007) proposed to increase the path loss between two nodes through adding the extra path loss caused by the obstacle. Therefore, assuming an obstacle between node i and node j, path loss can be computed as

$$PL(d,\theta,\zeta_{i,j}) = (PL(d_0) + 10\eta \log_{10}\left(\frac{d}{d_0}\right) + \zeta_{i,j}) \cdot K_\theta + N(0,\sigma_{ch}) \quad (11)$$

where $\zeta_{i,j}$ is the path loss caused by the obstacle between node i and j.

Radio irregularity affects the signal relationship between nodes. For example, in Fig. 4, if the circles indicate the distance at which the received signal power equals -100 dBm, node i and j can receive this power from each other. However, when radio irregularity is applied, the received signal power receivable at node j increases, and the received signal power receivable at node i reduces. Radio irregularity also affects channel access mechanisms. For example, in Fig. 4, node i cannot sense an ongoing transmission of node j, assuming the carrier-sensing threshold is -100 dBm. Therefore, although carrier sensing without modeling radio irregularity could avoid collision at node k, radio irregularity affects the carrier-sensing capability of node i and causes collision at node k.

3.6. Transmission power and noise floor heterogeneity

Transmission power heterogeneity indicates that for identical transmission power configurations the average transmission power of the nodes are different. Similarly, identical node types present different noise floors (Srinivasan et al., 2010; Ganesan et al., 2002; Cerpa et al., 2005; Zhou et al., 2006; Zamalloa and Krishnamachari, 2007). While the main reason behind this phenomenon is the manufacturing process, various battery level of the nodes also affect transmission power variations. Transmission power and noise floor heterogeneity are usually referred to as *hardware heterogeneity*.

The empirical results of Zamalloa and Krishnamachari (2007) and Srinivasan et al. (2010) revealed that transmission power and noise floor are correlated in Mica2 nodes. For example, for a given wireless node, higher positive deviation from the default transmission power is correlated with lower noise floor. The technical reason is that, if the transceiver chip has lower thermal noise, and the gain of the circuit between chip and antenna is high, that wireless node shows higher transmission power and lower noise floor. In order to consider the observed correlations, the multivariate Gaussian distribution has been used in the following form (Zamalloa and Krishnamachari, 2007):

$$\begin{pmatrix} \Omega_i^{adj} \\ \overline{\Psi}_i^{adj} \end{pmatrix} \sim N\left(\begin{pmatrix} \Omega_i \\ \overline{\Psi} \end{pmatrix}, \begin{pmatrix} (\sigma_{tx})^2 & C_{tx,rx} \\ C_{tx,rx} & (\sigma_{rx})^2 \end{pmatrix} \right) \quad (12)$$

where σ_{tx} is the standard deviation of transmission power heterogeneity, σ_{rx} is the standard deviation of noise floor heterogeneity, $C_{tx,rx}$ is the correlation between transmission power variance and noise floor variance, Ω_i^{adj} is the adjusted transmission power for node i, and $\overline{\Psi}_i^{adj}$ is the adjusted noise floor for node i. In terms of implementation, the Cholesky decomposition can be used to evaluate the above equation. It is worth noting that $\overline{\Psi}_i^{adj}$ should be substituted in Eq. (3) to obtain the noise power at a specific time. Among the network simulators, only TOSSIM (2014) models hardware heterogeneity. The followings are the values used by this simulator:

$$\text{Low Asymmetry}: \begin{pmatrix} 1.2 & -0.7 \\ -0.7 & 0.9 \end{pmatrix}$$
$$\text{High Asymmetry}: \begin{pmatrix} 6 & -3.3 \\ -3.3 & 3.7 \end{pmatrix} \quad (13)$$

In this paper, we refer to the packet reception variations caused by multipath, white Gaussian noise, noise heterogeneity and transmission power heterogeneity as the *system variations*, and it is represented as $[\sigma_{ch}; \sigma_{WGN}; \sigma_{tx}; \sigma_{rx}]$.

As hardware heterogeneity influences both transmission power and noise floor, its effects on network performance can be analyzed with respect to the discussions given for noise floor and radio irregularity.

3.7. Inter-node interference

As the wireless channel is a broadcast medium, each node's transmission affects other nodes' packet reception performance, depending on the distance from the receiver. Assume node j is sending a packet to node i. Also assume node k has node i in its propagation range, and its transmission is overlapped with the transmission time of node j, partially or completely. In this case, the signal sent by node k is considered as an interfering signal, regardless of its destination address. Let $\Upsilon_{j\to i}$ be the set of the

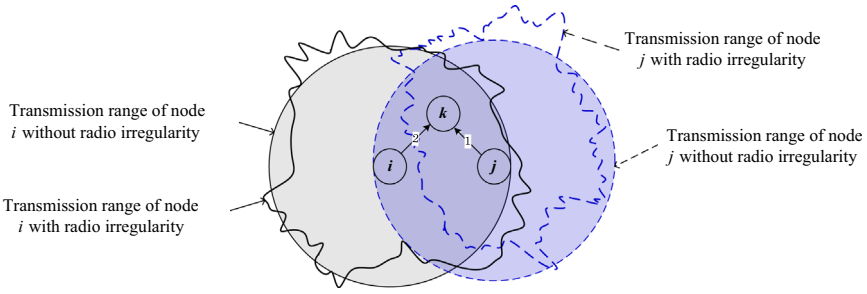

Fig. 4. Radio irregularity changes the signal relationship between nodes. This figure shows how radio irregularity affects the performance of MAC protocols.

nodes that their transmission time overlaps (fully or partially) with the packet reception from node j at node i. Then, $\Upsilon_{j\to i}\backslash\{j\}$ is the set of the interfering nodes for packet reception at node i from node j. This definition can easily be extended for broadcast transmissions.

The main difference between the interference models is the way they define interferer links and their effects on packet reception. Therefore, interference modeling highly affects packet reception performance, which reflects in network capacity and the operation of network protocols (Iyer et al., 2009; Li, 2009; Gupta and Kumar, 2000; Li et al., 2001). In this section, we investigate the five main interference models used in the literature: (i) *link quality model*, (ii) *interference range model*, (iii) *protocol model*, (iv) *capture threshold model*, and (v) *signal-to-interference-plus-noise ratio (SINR) model*.

3.7.1. Link quality model

This model utilizes the packet reception probabilities of the sender–receiver link and interferer–receiver links to estimate the probability of collision (Woo et al., 2003). With this model, the probability of successful packet transmission from node j to node i is given by

$$\gamma_{j,i}\times\prod_{k\in\Upsilon_{j\to i}\backslash\{j\}}(1-\gamma_{k,i}) \tag{14}$$

where $\gamma_{x,y}$ is the link quality between node x and node y. The link quality between two nodes can be computed using the *minimum transmission* (MT) metric (Woo et al., 2003) or *expected transmissions* (ETX) metric (Couto et al., 2005).

3.7.2. Interference range model

This model assumes two fixed circular ranges for packet reception and interference. The interference range is also referred to as the *carrier-sensing range* because it indicates the range within which a node's transmission can be detected (Iyer et al., 2009; Jung and Vaidya, 2002). With this model, node i can correctly receive from node j if,

$$d_{j,i}\le d_{com}\quad\text{and}\quad d_{k,i}\ge d_{intf}\quad\forall k\in\Upsilon_{j\to i}\backslash\{j\} \tag{15}$$

where $d_{x,y}$ refers to the Euclidean distance between node x and node y, d_{com} is the communication range, and d_{intf} is the interference range.

3.7.3. Protocol model

This model defines the condition of correct packet reception as follows (Gupta and Kumar, 2000; Cardieri, 2010; Wang et al., 2006):

$$d_{j,i}\le d_{com}\quad\text{and}\quad d_{k,i}\ge(1+\delta)d_{j,i}\quad\forall k\in\Upsilon_{j\to i}\backslash\{j\} \tag{16}$$

where $\delta>0$ and it determines the interference guard zone.

The major drawback of the interference range model and protocol model is that they cannot account for the accumulative effects of interference. In other words, node i can correctly receive the packet sent by node j regardless of the number of interfering nodes outside its interference range. However, this is in contrast with the observations reported by Blough et al. (2009), Iyer et al. (2009), Maheshwari et al. (2008a), and Ji et al. (2004).

3.7.4. Capture threshold model

This model uses three threshold values: (i) *RxThresh* as the reception threshold, (ii) *CpThresh* as the capture threshold, and (iii) *CsThresh* as the carrier-sensing threshold (NS-2, 2014). The signal transmitted by node j can be correctly received at node i if the following conditions hold:

$$\Psi(S_j)\ge\text{RxThresh},\quad\text{and} \tag{17a}$$

$$\frac{\Psi(S_j)}{\Psi(S_k)}\ge\text{CpThresh}\quad\forall k\in\Upsilon_{j\to i}\backslash\{j\} \tag{17b}$$

where $\Psi(S_x)$ refers to the reception power corresponding to the signal transmitted by node x. Although the capture threshold model is used in the simulators such as NS2 CTM (NS-2, 2014; Chen et al., 2007; Iyer et al., 2009) and GTNetS (Riley;GTNetS, 2013), it exhibits the same deficiency of the interference range model and protocol model: The received signal is compared with one interfering signal at a time, and the aggregate effect of interference is neglected. The second disadvantage of this model is that it cannot be combined with probabilistic packet reception algorithms. For example, assuming there is no interference, a packet can always be successfully received if its signal power is higher than RxThresh.

3.7.5. Signal-to-Interference-plus-Noise Ratio (SINR) model

This model, which is also called the *physical model* (Gupta and Kumar, 2000; Cardieri, 2010), utilizes the summation of the interfering signals and defines packet reception success as follows:

$$SINR_i(S_j)=\frac{\Psi_i(S_j)}{(\overline{\Psi}+\sum_{k\in\Upsilon_{j\to i}\backslash\{j\}}\Psi_i(S_k))}\ge SINR_{th} \tag{18}$$

where $SINR_i(S_j)$ is the *SINR* value at node i corresponding to the signal sent by node j, and $SINR_{th}$ is the minimum required *SINR* value for successful packet reception. Although $SINR_{th}$ in simulators such as NS2 has been set based on the empirical measurements (Iyer et al., 2009; Zhang et al., 2007; Reis et al., 2006; Chen et al., 2007; Lee et al., 2010a), Eq. (6) can be used to determine the $SINR_{th}$ required for achieving a specific packet reception ratio for a given network configuration. More importantly, instead of a threshold-based packet reception decision, SINR value can be substituted in a bit error rate model (e.g., Eq. (4)), from which the probability of successful packet reception can be obtained.

Son et al. (2006) have evaluated the accuracy of the SINR model with Mica2 nodes and they showed that the measured interference intensity is slightly lower than the addition of interfering signals. However, Maheshwari et al. (2008a, 2008b) demonstrated that SINR value only depends on the strength of the received signals, and the non-additive results presented by Son et al. are due to the hardware and measurement noise. The studies of Iyer et al. (2009), Halkes and Langendoen (2010), and Lee et al. (2010a) also confirm the highest accuracy of the SINR model.

3.8. External interference

External interference (a.k.a., *environmental interference*) refers to the signals produced by the sources outside of the network. Since 802.15.4, 802.15.1 and more importantly, 802.11b networks operate in the 2.4 GHz frequency band, the transmissions of the 802.15.4-compliant radios (such as CC2420) may highly be affected by external interference. Using CC2420 transceiver, Srinivasan et al. (2010) performed experimental analyses and they showed that 802.11 and 802.15.1 networks can significantly affect 802.15.4 transmissions. In addition, due to the higher power of 802.11b nodes, their MAC protocol does not perform backoff when 802.15.4 nodes are communicating. Therefore, 802.11b sources can result in spatially correlated packet losses with 802.15.4 transmissions. Their results reveal that only channel 26 of the 802.15.4 standard is immune against this interference. These observations suggest that protocol designers should consider the effects of external interference when the configured channel is not 26, or when a multi-channel MAC protocol is in use. For Bluetooth interference, Srinivasan et al. reported similar observations. However, the interference is slightly lower due to the frequency hopping mechanism of Bluetooth.

Lee et al. (2007c) also showed that the packet-based interference caused by 802.11 networks brings about correlated strong and short spikes. In order to simulate this interference, they have gathered noise traces in different environments using 802.15.4 nodes. The authors have proposed the following three approaches to produce statistical models from the gathered traces: (i) *naive sampling*, (ii) *closest-fit pattern matching* (CPM), and (iii) *a non-Gaussian random process*. In the naive sampling approach, the distribution of the gathered noise trace is computed and used whenever a noise value is required. Although this technique can provide noise samples in a fast and easy way, it does not include the correlation between noise values. In the CPM approach (implemented in TOSSIM), the first k generated noise samples are the k first samples obtained from the environment. Afterwards, in order to calculate noise value n_t, CPM samples from the PDF associated with n_{t-1}, $n_{t-2}, \ldots, n_{t-k}$, given the k previous values. CPM samples from the most common PDF if there is no associated PDF. As the value of k increases, CPM can capture longer correlations. However, k cannot be increased arbitrarily, because the state space grows as a^k, where a is the number of possible noise values. The third approach generates a non-Gaussian random process with a prescribed auto-correlation function to capture long-term correlations. Among these approaches, it has been shown that CPM has highest similarity to the real noise traces. While CPM can be effectively utilized to simulate the effects of external interference on the packet reception ratio between two nodes, this method has the following requirement and concern: The environment should be sampled to generate real noise traces to be fed into the CPM model. In addition, although Lee et al. present $k=20$ as the optimal value for their sampled environment, they have also mentioned that this may not be the optimal value for other cases.

Table 5
Simulation parameters.

Parameter	Value
Radio	
Average noise power [dBm]	−106
Noise figure [dB]	13
Switch to TX/RX [μs]	250
Radio sampling [μs]	350
Evaluate radio sample [μs]	100
Noise bandwidth [Hz]	30,000
Modulation	NC-FSK
Encoding	Manchester
Baud rate [Bauds per second]	38,400
Radio speed after encoding (R) [bps]	19,200
Transmission power [dBm]	0
Reference distance (d_0) [m]	1
PL(d_0) [dB]	55
White Gaussian noise (σ_{WGN}) [dB]	4
Transmission power heterogeneity (σ_{tx}) [dB]	1.2
Noise floor heterogeneity (σ_{rx}) [dB]	0.9
Correlation of transmission power and noise floor ($C_{tx,rx}$)	−0.7
Environment	
Path-loss exponent (η) (outdoor)	4.7
Multipath channel variations (σ_{ch}) (outdoor)	3.2
MAC	
Contention window [slot]	32
B-MAC sleep interval [ms]	30
Carrier-sensing threshold [dBm]	CCA
Packet format	
Physical header [byte]	8
MAC header [byte]	5
Payload [byte]	29
CRC [byte]	2

4. Methodology of performance evaluation

Since the rest of this paper presents performance evaluation results through simulation and empirical experimentation, in this section we overview the methodology used for performance evaluations.

We used the models presented in Section 3, the improved packet reception algorithm of Section 6.2, and the architecture proposed in Section 7.2 to develop a sophisticated simulation tool on the OMNeT++ simulation framework (OMNeT++, 2014). Although the models of this paper, and in particular, the architecture proposed in Section 7.2 can be used for accuracy improvement of various simulation tools, we employed OMNeT++ because it provides all the functionalities required to develop a new simulation tool. Therefore, if we wanted to use a simulator such as NS2, then we had to stick to its existing architecture and modify many modules.

The general simulation parameters of this paper are given in Table 5. The radio parameters have been chosen based on the documentation and empirical measurements of Mica2 motes with CC1000 radio. The implementation of CSMA and B-MAC are similar to that used in TinyOS (Levis et al., 2005; Polastre et al., 2004).

Table 6 summarizes the networks used in the evaluations of this paper. For 400-node networks, nodes are uniformly scattered in a square area. Each simulation run uses a unique seed value. Therefore, as we employed random network topology for N400HD, N400MD and N400LD, network topologies are different for various repetitions. The smaller network size used for validating the simulation results against empirical results is deployed in a grid form. The experiments are conducted in a typical outdoor environment.

Each figure point is the median of 20 runs. We also report the upper and lower quartiles for each point. To find the appropriate number of runs we increased the number of repetitions in 5-run steps. When the number of runs was higher than 20, we observed less than 10% change in the variance of the results.

4.1. Traffic patterns and evaluation metrics

We employ two traffic types in our performance evaluations: broadcast and convergecast. These traffic patterns are observable in the common applications of wireless sensor networks.

Table 6
Networks used in the evaluations of this paper.

Sections that use this network	Network name	Area ($m \times m$)	Number of nodes	Average number of neighbors per Node	topology
Sections 5.1, 5.2, 7.3.2	N400HD	40 × 40	400	40 (high density)	Random (uniform)
	N400MD	60 × 60	400	20 (medium density)	Random (uniform)
	N400LD	80 × 80	400	10 (low density)	Random (uniform)
Section 6.4	N36	6 × 16	36	Variable	Grid

With the broadcast traffic pattern, a packet sent by a node should be received by its neighbors. This traffic pattern is utilized during the initialization phases of wireless sensor networks: *neighbor discovery and link estimation* (NDLE) phase, and *collection tree construction* (CTC) phase (Dezfouli et al., 2014; Radi et al., 2013). For example, during the NDLE phase, each node broadcasts a fixed number of beacon packets and records the number of received beacons from its neighbors. Therefore, nodes can identify their neighbors and measure their corresponding link quality. We employ three types of broadcast scenarios:

- *Low-interference broadcast*: Each node generates a packet every 5 s, and sends the packet using the CSMA MAC protocol.
- *High-interference broadcast*: Each node generates and broadcasts its packets as fast as the CSMA channel access mechanism allows.
- *Fixed-interval broadcast*: Each node broadcasts a packet after a predetermined interval. Note that in contrast to low-interference broadcast, this traffic pattern does not employ CSMA.

In all the broadcast traffic scenarios each node sends 50 packets. Using the broadcast traffic pattern, we measure the following metrics:

- *Effective throughput*: Indicates the total number of correctly received packets at the nodes per second.
- *Number of hidden-node collisions*: A hidden-node collision happens when the radio is synchronized with an incoming signal, but a newly arrived signal corrupts the first signal.
- *RMSE*: Indicates NDLE accuracy, which is represented as $RMSE = \sqrt{(\sum_{i=1}^{N}(l_i - e_i)^2)/N}$, where N is the number of links, l_i is the average quality of link i, and e_i is the estimated quality of link i.
- *Number of discovered neighbors*: The average number of discovered neighbors per node.
- *Receptions*: Indicates the number of packets successfully received by the nodes.

The most well-known application of sensor networks is to send their sensed data towards a common sink node (Dezfouli et al., 2011; Ahn et al., 2006). This many-to-one traffic pattern is referred to as convergecast. Since the energy efficiency of this phase is critical, B-MAC (Polastre et al., 2004) is used as the MAC protocol. In addition, evaluations with this traffic pattern are conducted with the 400-node networks. We employ two types of convergecast scenarios:

- *Low-interference convergecast*: Each of the 20 nodes at the farthest distance from the sink node generate a packet every 5 min. Note that the sink node is located at the top left corner of the network.
- *High-interference convergecast*: Each node generates a packet every 30 s.

The following metrics are evaluated with the convergecast traffic pattern:

- *Packet delivery ratio*: The ratio of the received packets at sink to the total number of generated packets.
- *Average end-to-end delay*: The average packet delay from packet generation until reception at sink.
- *Average number of hops*: The average number of hops traversed by the packets to reach the sink node.

Notice that convergecast requires the nodes to be aware of their paths towards the sink. In this paper, we assume that nodes have established a data-gathering tree during the initialization phase using the Collection Tree Protocol (CTP) (Gnawali et al., 2013). In addition, in order to eliminate the negative effects of NDLE accuracy on data gathering performance, we run a high-accuracy NDLE protocol before data gathering.

5. Analyzing the importance and effects of system variations and radio irregularity

In this section, we consider real applications of large-scale sensor networks to: (i) show the effects of system variations and radio irregularity on the performance of MAC, link estimation, routing and network energy consumption; (ii) confirm the importance of modeling system variations and radio irregularity for performance evaluations.

5.1. Network performance versus system variations

In this section, we analyze the influence of system variations on the performance of wireless sensor networks. Instead of hardware heterogeneity (link asymmetry), we specifically focus on the effects of transitional region size (link unreliability) variations caused by multipath and white Gaussian noise. The analyses of this section reveal the unavoidably important performance effects of link unreliability.

5.1.1. Broadcast traffic

We show the effects of system variations in low-interference and high-interference broadcast scenarios in Fig. 5. Notice that configuration [0;0;0;0] corresponds to the unit disk graph (UDG) model, which does not represent link variation and asymmetry. These results show that transitional region enlargement and hardware heterogeneity cause lower throughput and higher number of hidden-node collisions. Through increasing the transitional region size, we effectively extend the interference range of the nodes. In particular, while extending the transitional region improves the probability of packet reception at longer distances, it does not improve the carrier-sensing efficiency of the MAC protocol (which is required for collision avoidance). On the other hand, since expanding the transitional region causes larger neighborhood size, it increases the chance of selecting a backoff slot by at least two nodes; hence, outcomes in higher packet losses. Beside the effects of transitional region on carrier-sensing performance, hardware heterogeneity also reduces the efficiency of CSMA because it increases the number of asymmetric links.

Figure 6 shows how increasing link unreliability reflects in NDLE accuracy. While the low-interference broadcast scenario provides significantly better link estimation accuracy (through providing lower RMSE), our results also show that larger transitional region reduces the accuracy of link estimation. As stated earlier, larger transitional region and hardware heterogeneity intensify the number of collisions, which in turn reduces the number of packet receptions required for link estimation. Furthermore, although packet reception ratio in the connected region is higher than 90% and most of the links in this region can be perfectly estimated, links in the transitional region are much more prone to signal variations and collision; therefore, these links cannot be well estimated. Accordingly, increasing system variations reduces link estimation accuracy, because it enlarges the ratio of the links in the transitional region to those links in the connected region (cf. Section 3.1, Fig. 2). Since most of the routing protocols rely on link estimation (Radi et al., 2011, 2012), these results reveal the potential influence of system variations on the performance of routing protocols.

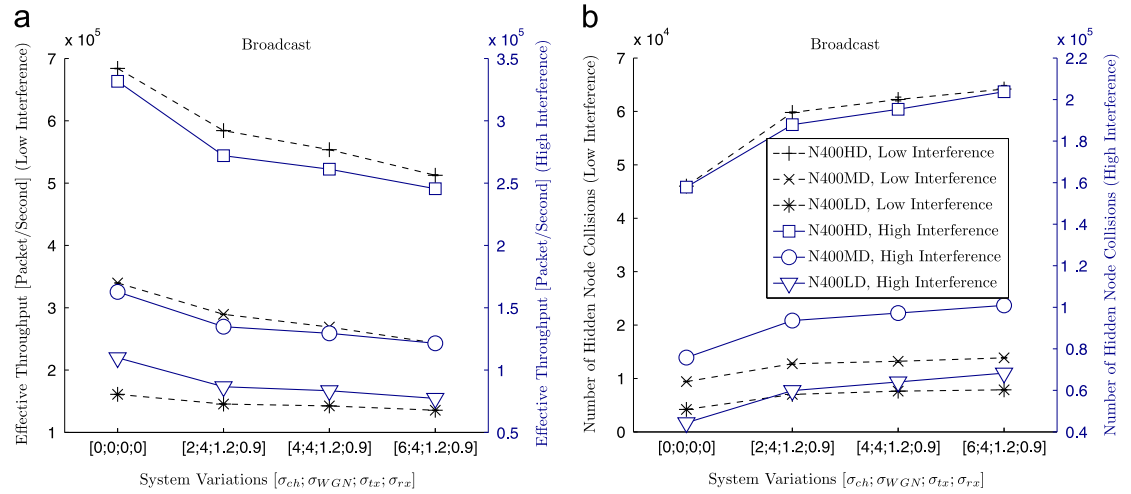

Fig. 5. Effects of system variations on the performance of packet broadcast. (a) Effective throughput; (b) number of hidden-node collisions. Increasing the system variations generates more number of unreliable links, increases the interference distance, reduces the efficiency of carrier sensing, and results in higher packet corruptions.

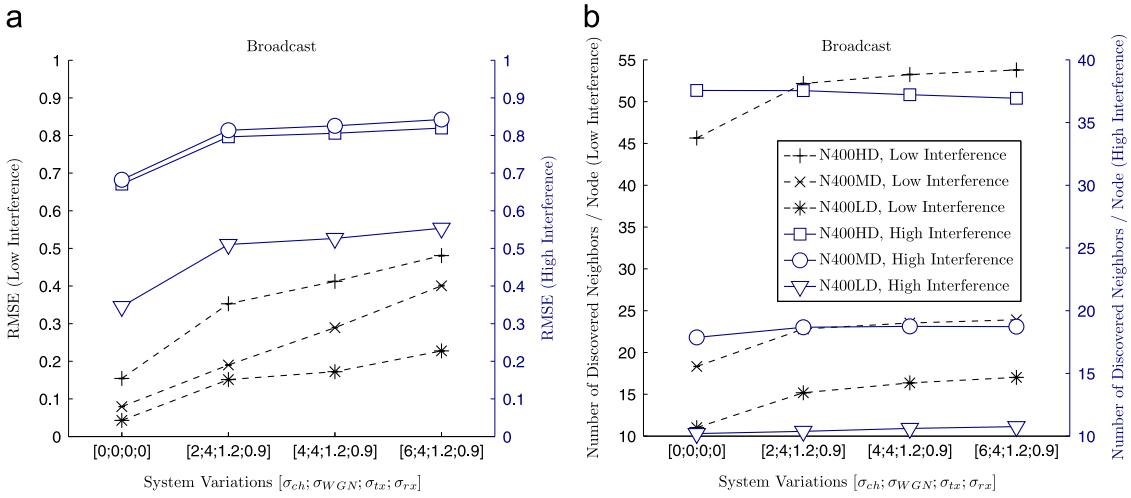

Fig. 6. Effects of system variations on the accuracy of NDLE. (a) Link estimation accuracy (RMSE); (b) average number of discovered neighbors per node. While system variations highly affect NDLE performance, these effects specifically reflect in the performance of routing protocols.

As stated earlier, although enlarging the transitional region improves the chance of packet reception at longer distances, it also causes higher collision intensity and reduces the chance of packet reception from neighbors. However, due to the lower number of collisions in the low-interference scenario, the influence of larger transitional region on this scenario is the higher number of discovered neighbors.

5.1.2. Convergecast traffic

Figure 7 shows our performance evaluations with the convergecast traffic pattern. The main observation of these results is that transitional region enlargement and hardware heterogeneity reduce the data-gathering performance. This behavior is due to the underlying collection tree structure, which determines each node's path towards the sink. Specifically, since increasing link variations reduces the connected region size, the Collection Tree Protocol (which utilizes link qualities as its path metric) employs shorter hops to satisfy path quality. The direct effects of this change are: longer paths towards the sink, higher probability of packet loss along the source-destination paths, and higher end-to-end delay. In terms of energy consumption, although longer paths demand higher energy consumption for packet forwarding, nevertheless, it results in lower energy consumption, because it also outcomes in higher packet loss ratio. For example, when we changed the system variations from [0;0;0;0] to [6;4;1.2;0.9], we observed up to 40% reduction in the average energy consumption of the nodes. We did not present the energy measurement results due to space limitations.

5.2. Network performance versus radio anisotropy

In this section, we analyze the effects of radio irregularity (link asymmetry) on the performance of wireless sensor networks. It is worth mentioning that the results presented in this section are complementary to the results of Zhou et al. (2006), which have been reported for 802.11 networks.

5.2.1. Broadcast traffic

Figure 8 shows the effects of radio irregularity on the performance of broadcast traffic. For both traffic scenarios, increasing the DOI value results in a higher number of hidden-node collisions, which is due to the lower efficiency of carrier sensing with higher link asymmetry. Although radio irregularity causes significant changes on network throughput, our results indicate slight increase

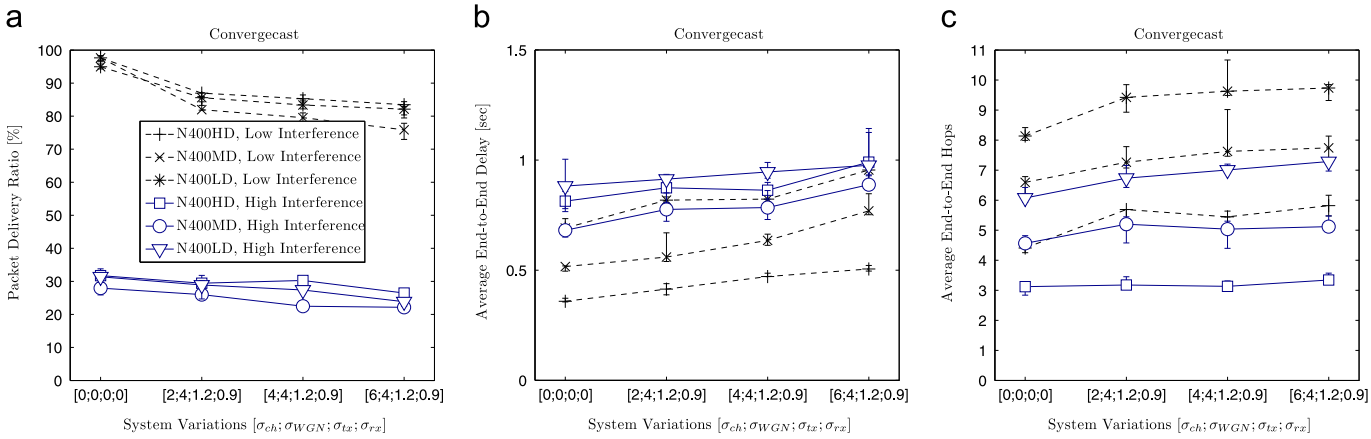

Fig. 7. Effects of system variations on data gathering performance. (a) Packet delivery ratio; (b) average end-to-end packet delay; (c) average number of end-to-end hops. Increasing system variations reduces the efficiency of data-gathering applications due to the effects on MAC and routing protocols. The performance reduction is specifically caused by the higher number of hops, larger interference range, and lower carrier-sensing efficiency.

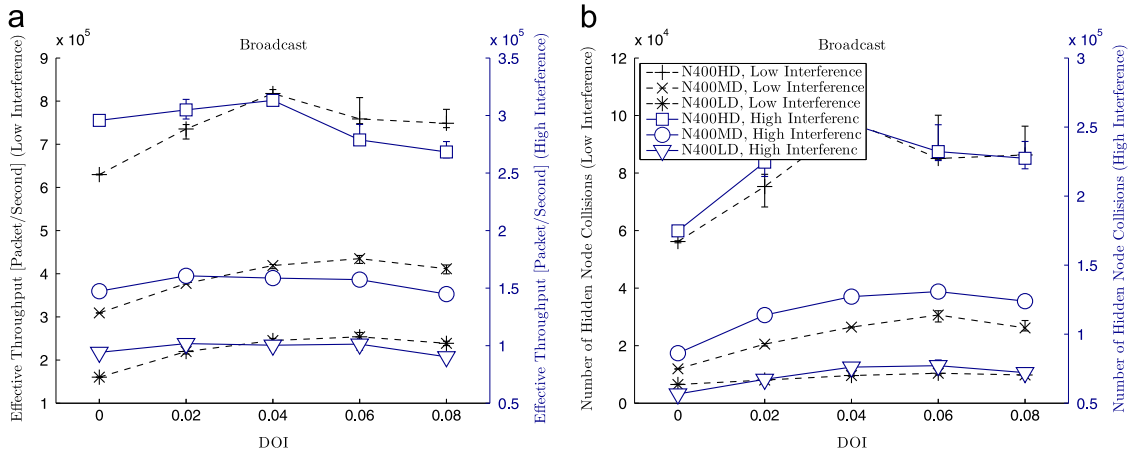

Fig. 8. Effects of radio irregularity on the performance of packet broadcast. (a) Effective throughput; (b) number of hidden-node collisions.

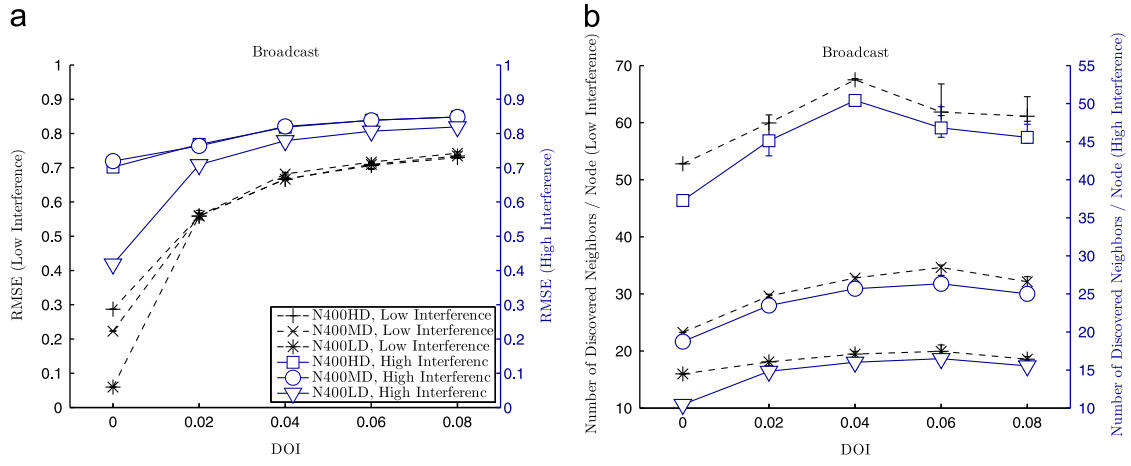

Fig. 9. Effects of radio irregularity on the accuracy of link estimation and neighbor discovery. (a) Link estimation accuracy (RMSE); (b) average number of discovered neighbors per node. Radio irregularity significantly affects NDLE performance, which also reflects in the performance of MAC and routing protocols.

and slight decrease in the number of packet receptions for the low and high-interference scenarios, respectively. As demonstrated in Section 3.1, a minor decrease in path-loss exponent causes significant increase in transitional region size. Accordingly, radio irregularity causes considerable extension of the transitional region at some directions (Fig. 3). Therefore, in the low-interference scenario, in which the number of hidden-node collisions is low, radio irregularity increases the number of packet receptions at longer distances. On the other hand, when the interference intensity is high, the effects of hidden-node collisions is higher than that of transitional region extension; therefore, it reduces the number of receptions.

Figure 9 shows that radio irregularity significantly affects link quality estimation. This is due to two reasons: (i) Assuming node *i* wants to measure its link quality to node *j*, node *i* requires

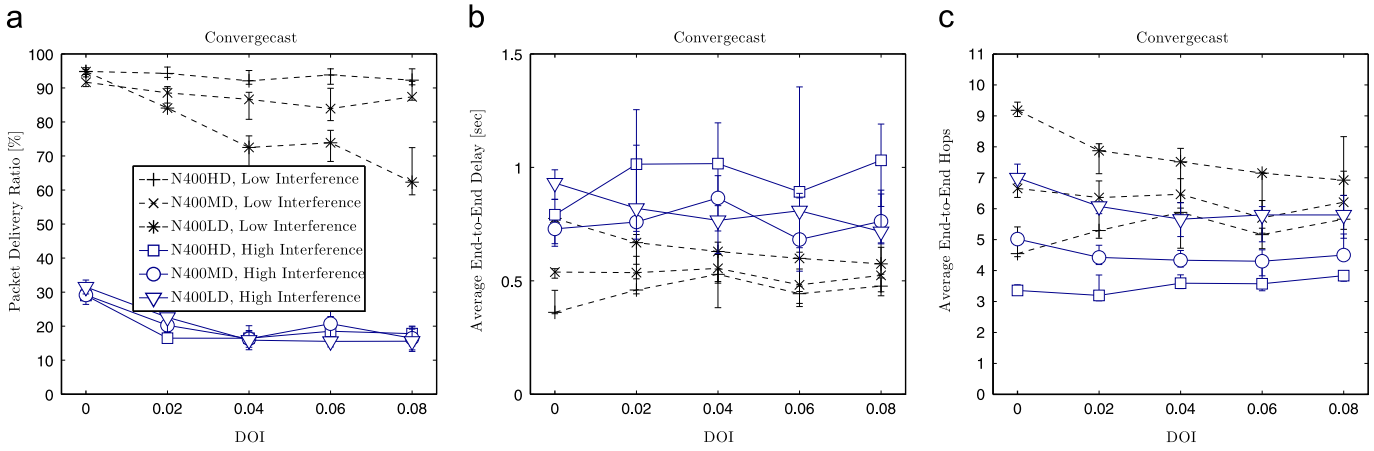

Fig. 10. Effects of radio irregularity on data-gathering performance. (a) Number of packet receptions at sink; (b) average end-to-end packet delay; (c) average number of end-to-end hops. Radio irregularity increases the number of packet losses, and reduces the number of packets delivered to the sink. Additionally, radio irregularity causes considerable variations in the length and quality of paths.

receiving packets from node *j* to measure the number of packets node *j* has successfully received from node *i*. Therefore, link asymmetry increases the inaccuracy of estimating forward links. (ii) The hidden-node collisions caused by radio irregularity reduce the number of packet exchanges between nodes. From the neighbor discovery point of view, radio irregularity causes considerable extension of the transitional region at some directions. Therefore, we can observe the increase in the average number of neighbors per node.

5.2.2. Convergecast traffic

Figure 10 shows how radio irregularity affects convergecast performance. Radio irregularity reduces the ratio of the delivered packets to the sink, which is due to the higher packet losses caused by collisions. Radio irregularity also affects end-to-end delay due to two reasons: (i) The higher packet losses changes the traffic pattern and channel access delay; (ii) Radio irregularity results in considerable changes in the paths towards the sink. The second reason can also be observed from Fig. 10(c), where the number of hops varies against DOI changes. It should be noted that radio irregularity does not necessarily result in lower or higher number of hops or delay. For example, if the extension in the transmission range is towards the sink node, the path passing through that node would become shorter. In contrast, a reduction in a node's transmission range may require that node to route its packets through a longer path. Radio irregularity also affects nodes' energy consumption due to the changes in the traffic pattern. When we changed DOI from 0 to 0.08, we observed that the packet losses caused by radio irregularity cause up to 40% reduction in the average energy consumption of the nodes.

6. Packet reception algorithms

A packet reception algorithm determines how the physical layer employs an interference model to decide about packet reception. Therefore, the employed interference model impacts the design and accuracy of the packet reception algorithm. Unfortunately, the packet reception algorithms utilized in the well-known simulators suffer from inaccuracies that cannot be neglected in evaluating low-power wireless networks. Here, we review the packet reception algorithms used in NS2. These analyses also hold for the simulators that employ similar packet reception algorithms. Next, we propose an improved packet reception algorithm that provides higher accuracy than the NS2 packet reception algorithms. We demonstrate the accuracy of this algorithm through comparison with empirical results.

6.1. Packet reception algorithms of NS2

We first evaluate the packet reception algorithm employed by NS2 CTM, in which the capture threshold model (cf. Section 3.7.4) is used as the interference model. This algorithms is referred to as CTMA (CTM-based Algorithm) in this paper. We have produced the state machine of this algorithm in Fig. 11.

When a sample signal S_i arrives at a node's physical layer, if there is no other signal available at the node (i.e., $\mathbf{S} = = \varnothing$), the received signal strength of this signal (i.e., $\Psi(S_i)$) is compared with RxThresh. The state machine moves from the *Searching* state to the *Receiving* state if inequality $\Psi(S_i) >$ RxThresh holds. If a new signal S_n arrives during the reception of signal S_i, inequality $\Psi(S_i)/\Psi(S_n) >$ CpThresh is evaluated. If this inequality holds, signal S_n is dropped and the packet reception algorithm continues with signal S_i; otherwise, both signals are dropped. The main drawbacks of this algorithm are as follows:

- This algorithm does not support stronger-last captures. To solve this problem, Inequality 17(a) and (b) should be evaluated whenever a new signal arrives during a packet reception.
- There is no difference between preamble reception and MPDU reception. Therefore, for example, if different bit rates are used for the preamble and MPDU, this model cannot reflect the differences in the probability of packet synchronization and MPDU reception.
- Due to the use of the capture threshold model, the aggregate effect of interference on packet reception is neglected.
- This algorithm neglects signal variations during packet reception.

The second evaluated packet reception algorithm is employed by NS2 SINR, in which the SINR model (cf. Section 3.7.5) is used. This algorithm is referred to as SINRA (SINR-based Algorithm) in this paper. SINRA is mainly proposed by Chen et al. (2007) after the observations reported in Chen et al. (2006) and Schmidt-eisenlohr et al. (2006). Figure 12 shows the state machine we have produced from the packet reception algorithm of this simulator.

The state machine is in the *Searching* state when there is no signal at the radio, or when the power of each signal is lower than the preamble detection threshold. If a signal arrives and its SINR is higher than the threshold value, the state machine changes into the *PreRXing* state. If this signal's SINR remains higher than the threshold value for the preamble duration, the state changes into the *RXing*, during which the MPDU should be received. If the signal

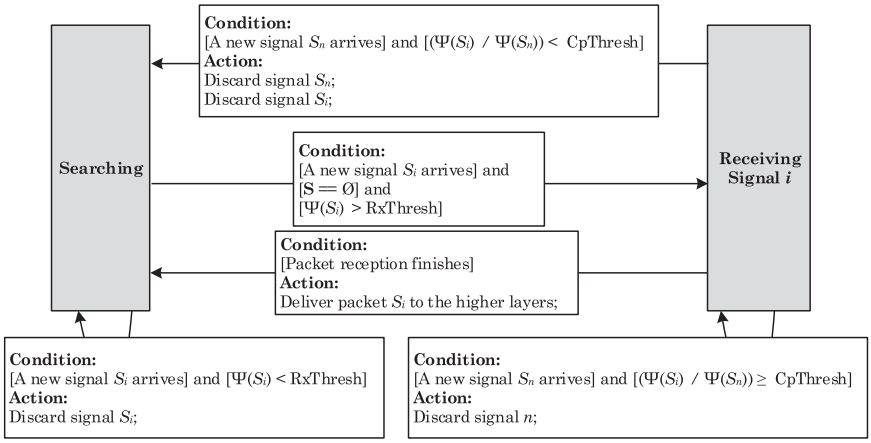

Fig. 11. The packet reception algorithm of NS2 CTM. The major drawbacks of CTMA are: (i) it does not consider additive interference; (ii) it does not model stronger-last captures; (iii) it cannot start a new packet reception when there is at least one other signal available; and (iv) it does not model signal synchronization.

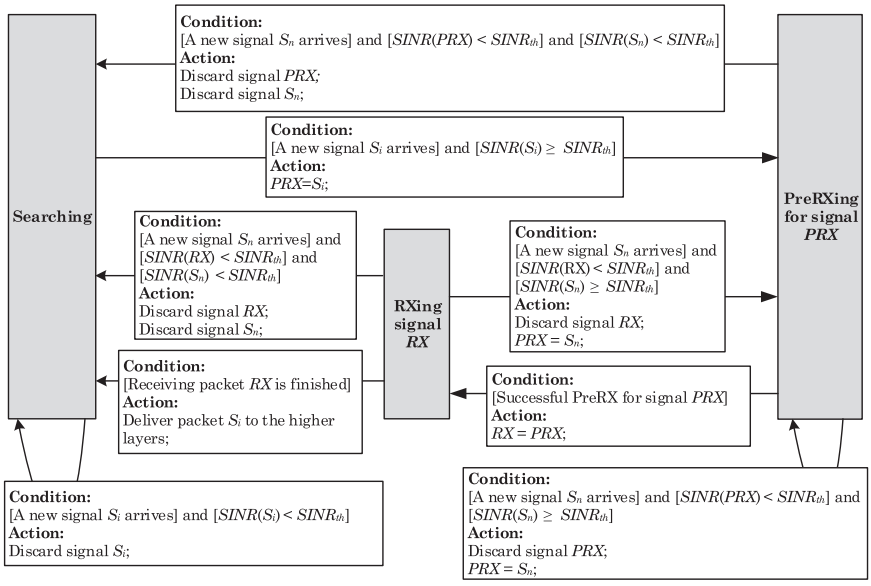

Fig. 12. The packet reception algorithm of NS2 SINR. The major drawbacks of SINRA are: (i) it does not provide accurate signal synchronization, because the main decision for packet reception is made at packet arrival; (ii) decision for packet reception is based on the threshold value.

power goes below the required threshold value during the MPDU reception, the packet is marked as erroneous. Arrival of a signal during the *PreRXing* or *RXing* states may start a new preamble reception duration if the new signal's SINR is higher than the threshold value. The drawbacks of this algorithm are as follows:

- Although this algorithm supports stronger-first and stronger-last captures, it goes into the *PreRXing* state if a signal's SINR value is higher than a certain threshold upon its arrival. Therefore, when the preamble size is larger than the settling bits, a packet cannot be received if it cannot provide enough SINR upon its arrival but its SINR value is large enough during the settling bits.
- Since SINR evaluations are performed at signal arrival times, signal variations during packet reception cannot be precisely modeled. In particular, instead of using a probabilistic packet reception model, threshold SINR values have been defined to decide about preamble and MPDU reception.

Unfortunately, the packet reception algorithm of NS3 is also similar to that of SINRA. Specifically, even with the improvements proposed by Al-Bado et al. (2012), the packet reception algorithm of NS3 cannot receive those packets with partially corrupted preamble.

6.2. An improved packet reception algorithm

In this section we propose the Capture Aware Reception Model (CARM) to overcome the inaccuracies of CTMA and SINRA. The state machine of this model is given in Fig. 13.

In contrast with SINRA in which decision for packet reception is made upon signal arrival, CARM performs continuous SINR evaluations to check whether a signal can be synchronized with the radio. To this aim, CARM requires managing two lists of signals:

- PreSYNC Signals: This list includes those signals that have not reached their settling bits. A signal in this list can be synchronized with the radio if it provides enough SINR during the settling bits.
- SYNC/MPDU Signals: This list includes those signals that their settling bits are being arrived or are finished. A signal of this list

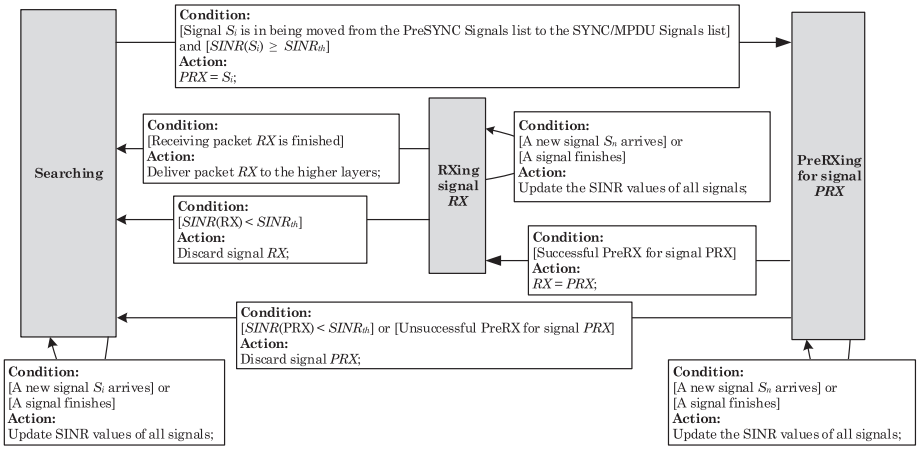

Fig. 13. The state machine of CARM. In addition to employing the SINR model, this algorithm also provides a realistic implementation of packet synchronization. Specifically, it supports packet reception when enough SINR cannot be sustained throughout the preamble duration. Therefore, this algorithm does not present the inaccuracies of CTMA and SINRA.

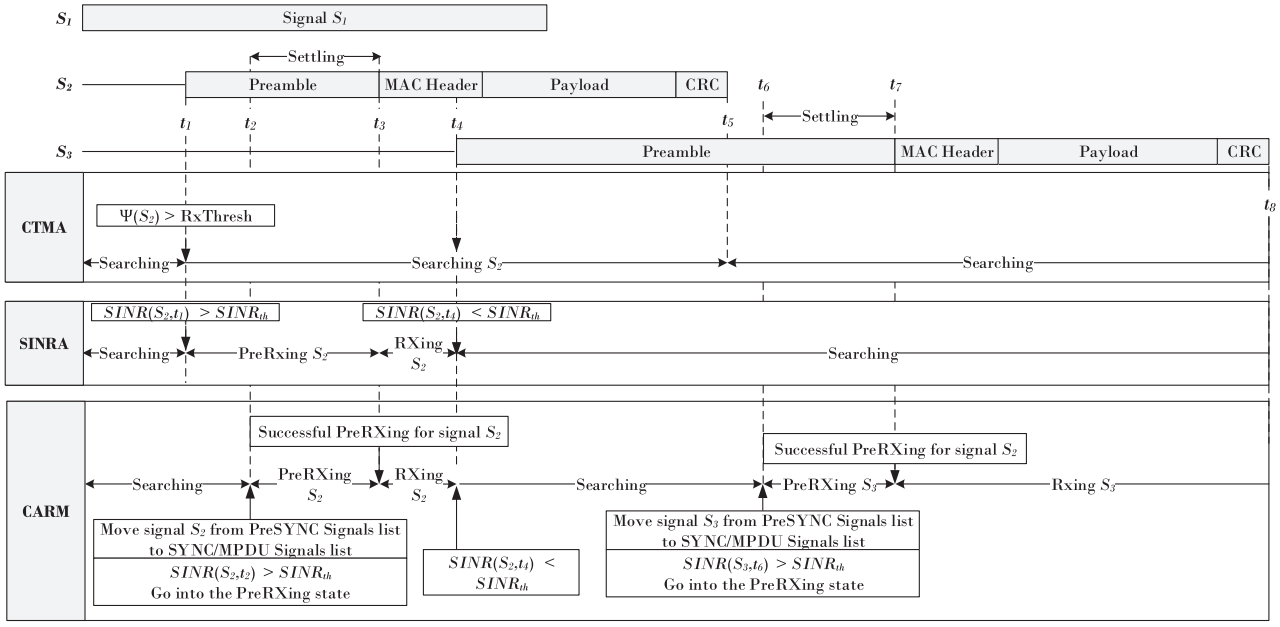

Fig. 14. A sample packet reception scenario to represent the operation of various packet reception algorithms. With respect to the signal powers, we assume: (i) packet S_1 should not be received; (ii) packet S_2 should be partially received (until t_4); (iii) packet S_3 should be completely received. CTMA and SINRA miss packet S_3. CARM partially receives packet S_2, and completely receives packet S_3. This scenario shows that CARM can model the real behavior of low-power wireless transceivers.

can be in one of the following states: (i) *PreRXing*: if its SINR value is higher than $SINR_{th}$ during the settling bits; (ii) *RXing*: if it has been successfully synchronized with the transceiver.

When the state machine is in the *Searching* state and a signal is being moved from the PreSYNC Signals list to the SYNC/MPDU Signals lists, CARM checks whether the SINR of this signal is high enough for synchronization. If yes, the state is changed to the *PreRXing* state, and CARM evaluates the correct reception of the settling bits of this signal. To evaluate the synchronization correctness, CARM samples the signal's SINR values during the settling bits, and uses these values to compute the correctness of receiving the settling bits. State machine goes into the *RXing* state if the reception of settling bits has been successful. When the state machine is in the *RXing* state, the receiving signal's SINR value is sampled as long as its SINR is higher than $SINR_{th}$. $SINR_{th}$ is the minimum SINR value required for receiving one byte.

6.3. Detailed analysis of a packet reception scenario

Figure 14 shows a sample packet reception scenario, which highlights the inaccuracies of the NS2 packet reception algorithms and presents the benefits of CARM over these models.

This figure shows the arrival of two signals at a sample node. We assume: (i) signal S_1's power is not enough for reception; (ii) signal S_2 can be received as long as signal S_3 has not arrived; (iii) signal S_3 can be completely received. Here we describe how the aforementioned packet reception algorithms behave in this scenario:

- CTMA: When signal S_2 arrives, although Inequality 17(a) holds, CTMA does not start a new packet reception because signal S_1 exists. Similarly, CTMA misses packet S_3.
- SINRA: When signal S_2 arrives, the SINR of this signal is measured (through Inequality 18), and the state changes into *PreRXing*. S_2's preamble can be successfully received, because

its SINR is higher than $SINR_{th}$ during t_1–t_3. The MPDU reception of this signal starts at t_3. However, when signal S_3 arrives, the state changes into the *Searching*, since the SINR of S_2 drops below the threshold value. Additionally, as the SINR of signal S_3 is lower than the threshold value upon its arrival, SINRA does not consider this packet for reception.

- CARM: The state machine of CARM does not perform state change at the arrival of signal S_2. However, at the beginning of the settling bits of signal S_2 (i.e., t_2), the SINR of this signal is evaluated and the state is changed to *PreRXing*. After successfully receiving the settling bits, the state is changed to *RXing* to receive S_2's MPDU bytes. The packet reception is halted at t_4 and the state is changed to *Searching*, since the SINR of S_2 goes below the threshold value. At time t_6, in which the settling bits of S_3 start, the SINR of this signal is evaluated and the reception of this packet is started. Accordingly, CARM does not present the inaccuracies of CTMA and SINRA.

6.4. Accuracy of the packet reception algorithms: simulation vs empirical results

In this section we measure the accuracy of CARM, CTMA and SINRA against the empirical results obtained from a 36-node Mica2 testbed deployed as a 9×4 grid. This network is referred to as N36 in Table 6. It is worth noting that we chose Mica2 because the characteristics of the CC1000 transceiver are well investigated by the literature, and this allowed us to match the simulation and empirical results through parameter calibration. In order to focus on packet reception accuracy, we use simulation platforms that only differ in terms of the employed packet reception algorithm. In particular, we have implemented CARM, CTMA and SINRA on the OMNeT++ simulation framework using the architecture proposed in Section 7.2. Therefore, the difference in the simulation results is only caused by the operation of the packet reception algorithm in use. To eliminate the effect of MAC mechanism on collision avoidance and packet reception performance, we used the *fixed-interval broadcast* scenario described in Section 4.1. Varying the broadcasting interval changes the collision intensity. Figure 15 shows the results.

As CARM does not represent the inaccuracies of the NS2 packet reception algorithms, it can achieve considerably higher accuracy compared with SINRA and CTMA. Specifically, while the accuracy of the NS2 packet reception algorithms depends on interference intensity, CARM's accuracy is very similar to that of the empirical results, regardless of interference intensity.

When the broadcast interval is short, collision intensity is very high and the number of packets that can provide enough SINR for successful reception is very low. However, when the broadcast interval is increased, interference intensity during packet receptions reduces, and in particular, the number of packets that cannot provide enough SINR during a specific duration of their reception

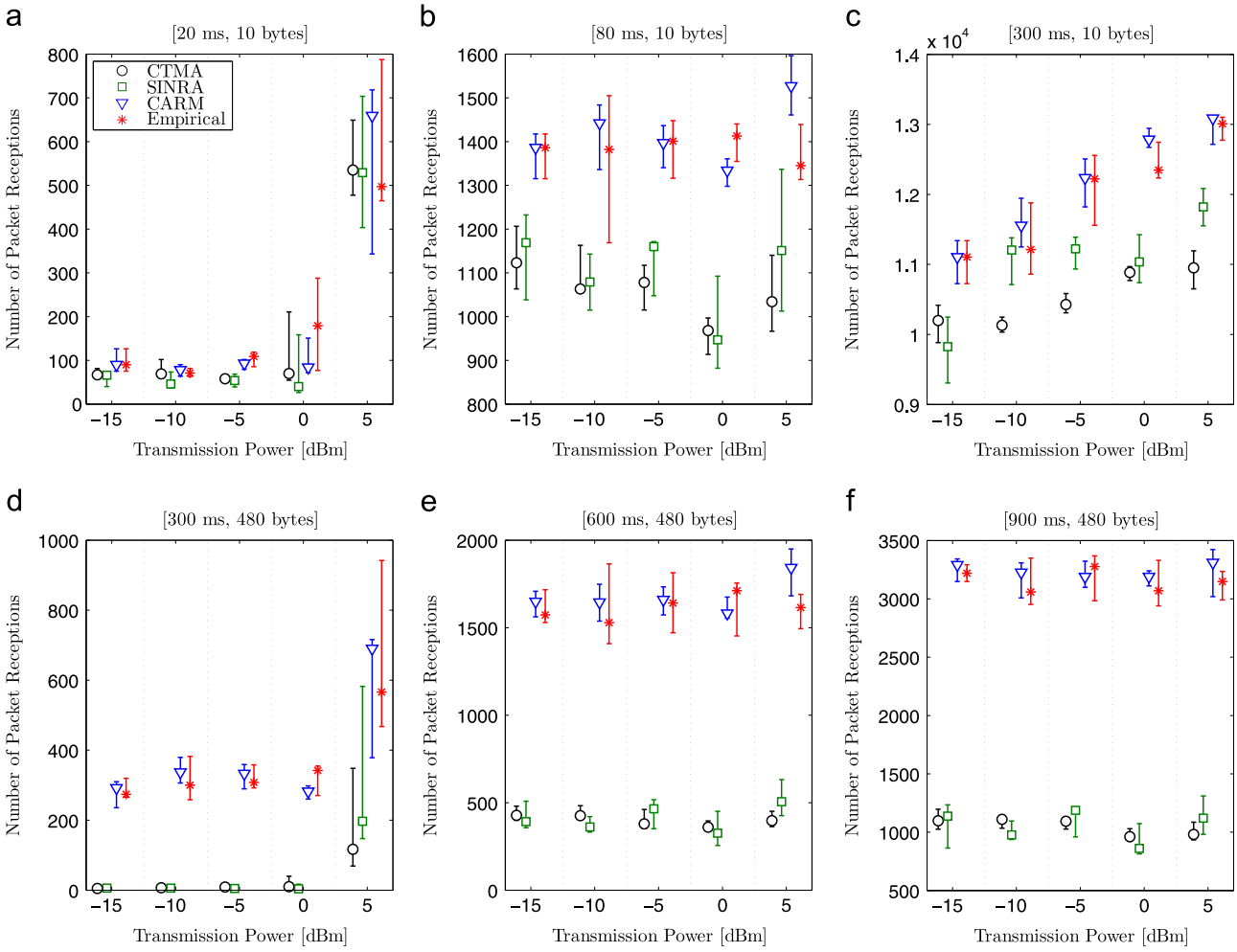

Fig. 15. Comparing the accuracy of CARM, CTMA and SINRA against empirical results. The two values above each figure represent broadcast interval and preamble size, respectively. These results clearly reveal the inaccuracy of CTMA and SINRA. While these packet reception algorithms adversely affect the simulation accuracy, CARM can achieve significant accuracy, especially when the preamble size is large.

increases. In other words, this increases the number of packets that their SINR value upon arrival is not enough for packet reception, but they can provide enough SINR during their settling bits (e.g., signal S_3 in Fig. 14). This condition reveals the inaccuracy of the NS2 packet reception algorithms, because the main decision made by these algorithms for packet reception is at the time of a new signal arrival. This can justify, for example, why the number of receptions achieved by SINRA and CTMA are considerably lower than that of CARM and empirical results (compare Fig. 15(b) and (a)). As enlarging the preamble size increases the number of packets that cannot provide enough SINR upon arrival but their SINR is enough during the settling bits, Fig. 15(d), (e) and (f) show higher inaccuracy for SINRA and CTMA compared with Fig. 15(a), (b) and (c).

Comparing Fig. 15(b) and (c) shows lower difference between the results of NS2 packet reception algorithms and empirical experiment. This can be justified as follows: when the preamble size is 10 bytes and the broadcast interval is increased from 80 ms to 300 ms, interference intensity is significantly reduced and the number of packets that can provide high SINR throughout their preamble duration increases.

7. Implementation and performance tradeoffs

In this section, first, we highlight the architectural shortcomings of NS2 SINR and NS2 CTM for implementing the essential models presented in this paper. Then, we propose an architecture within which all the essential models required for evaluating low-power wireless networks can be implemented. We also study the effect of each model on simulation speed. Afterwards, we investigate the effects of propagation range confinement, which is an important approach used by the simulation tools for improving simulation speed.

7.1. Architecture of NS2

None of the existing simulation tools implement all the essential models presented in this paper. Additionally, their architecture does not support straightforward addition of the mentioned models.

In N2 CTM, the *WirelessChannel* module connects all the nodes and takes care of packet exchange between them. Whenever a node sends a packet, the *WirelessChannel* module delivers a copy of that packet to the *WirelessPhy* module of all the nodes. Using the *RF Model* module, which implements the propagation model, the power of the received signal is computed, and the signal is passed to the MAC layer if its received power is higher than the carrier-sensing threshold. The architecture of NS2 SINR is very similar to that of NS2 CTM. However, the *WirelessPhy* has been replaced with a more sophisticated physical layer module, called *PHY*. Although NS2 SINR enhances simulation accuracy through employing an improved packet reception algorithm (cf. Section 6.1), the other characteristics of wireless communications have not been implemented. For example, none of these simulators support radio irregularity, hardware heterogeneity and propagation range optimization mechanisms.

7.2. An improved architecture

Figure 16 shows the proposed architecture, which supports the integration and implementation of the essential models presented in this paper. This architecture is composed of two main modules: *Wireless Channel* and *Physical Layer*. Whenever a node wants to send a packet, it should deliver that packet to the *Wireless Channel* module. The main responsibility of this module is to deliver a copy of the transmitted signal to the *Physical Layer* of the nodes in the propagation range of the sender.

The two main data structures of the *Wireless Channel* module are *Node Vector* and *In-Range Vector*. *Node Vector* is an array of size $|\mathbf{V}|$ elements, and each element stores some information about a specific node. The essential information stored at each element are node location, adjusted transmission power, and propagation range. There is an *In-Range Vector* for each entry of the *Node Vector*. An *In-Range Vector* includes those nodes that should be affected by the transmission of the node in the *Node Vector*. In order to construct the *In-Range Vectors*, the *Wireless Channel* module should compute the distance between all node pairs. Let $\mathbf{V}=\{V_1, V_2, \ldots, V_{|\mathbf{V}|}\}$ represent the set of the nodes in the network. In order to decide whether node V_j should be included in the *In-Range Vector* of node V_i, the *Wireless Channel* module computes $d_{i,j}$, which is the Euclidean distance between node V_i and V_j. If $d_{i,j} < d_{prop}$, an entry should be added to the *In-range Vector* of node V_i. We will investigate determining d_{prop} in Section 7.3.

As stated in Section 3.5, signal propagation around a transmitter is anisotropic. With respect to the characteristics of radio irregularity (i.e., anisotropy and continuous variations), we model radio irregularity at the *Wireless Channel* module as follows. First, since the received signal strength around a transmitter demonstrates continuous variations with respect to direction changes, we should compute K_θ values. In other words, we utilize Eq. (10) to compute 360 coefficient values for each entry of the *Node Vector*. To record the computed values, each entry of the *Node Vector* includes a 1×360 matrix, called *anisotropy matrix*, and denoted by **A**. Second, during the construction of the *In-Range Vectors*, for each node V_j in the *In-Range Vector* of node V_i, the degree of the vector passing through node V_i and V_j is required. Assume function

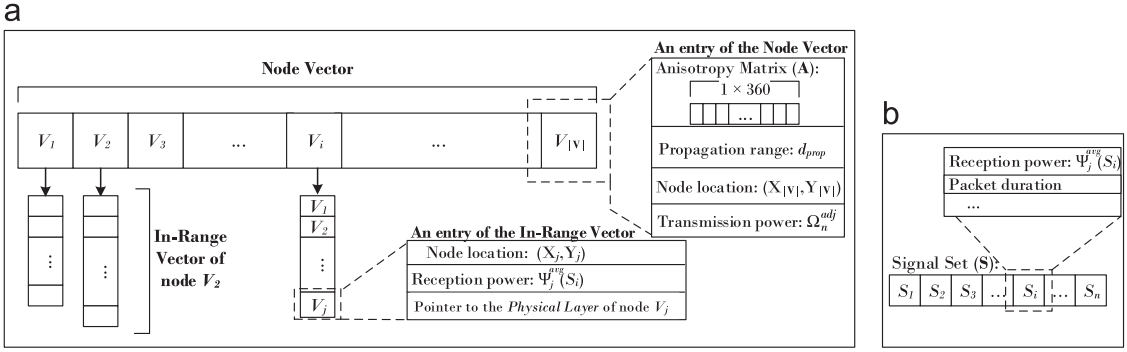

Fig. 16. The proposed architecture to implement the models required for accurate evaluation of low-power wireless networks. Transmission power heterogeneity, radio irregularity, and propagation range confinement are modeled at the *Wireless Channel* module. Multipath effect and white Gaussian noise are modeled in the *Physical Layer* module. The data structures of the *Wireless Channel* module, i.e., *Node Vector* and *In-Range Vector*, should be established once and no update is required unless there is node mobility or transmission power change. The *Physical Layer* of each node needs to update set **S** after the arrival and end of each signal.

$\theta(V_i, V_j)$ returns the degree of this vector, where $\theta(V_i, V_j) \in [0, 359]$. Using the models surveyed in Section 3, we combine the log-normal and RIM model to obtain the average reception power from node V_i at node V_j,

$$\Psi_j^{avg}(S_i) = \Omega_i^{adj} - \left(\left(PL(d_0) + 10\eta \log_{10}\left(\frac{d_{i,j}}{d_0}\right) \right) \cdot K_{\theta_{i,j}} + \zeta_{i,j} \right) \quad (19)$$

where $K_{\theta_{i,j}}$ is the path-loss coefficient obtained from the anisotropy matrix as $\mathbf{A}[\theta(V_i, V_j)]$, and $\zeta_{i,j} \neq 0$ if there is an obstacle between node i and j. For each node x in the *In-Range Vector* of node V_i, the *Wireless Channel* module should compute $\Psi_x^{avg}(S_i)$ and record its value.

While the *Wireless Channel* module implements transmission power heterogeneity and path-loss anisotropy, the influence of multipath channel and white Gaussian noise are modeled at the *Physical Layer* module. Assume the *Wireless Channel* module delivers the signal sent by node i to node j. The *Physical Layer* of node j computes the SINR value of signal S_i at time t as follows:

$$SINR_j(S_i, t) = \frac{\Psi'_j(S_i, t)}{\overline{\Psi}_j^{adj}(t) + \sum_{S_k \in \mathbf{S} \setminus \{S_i\}} \Psi'_j(S_k, t)} \quad (20)$$

where $\Psi'_j(S_x, t)$ is the received signal power plus multipath variations from node x, and it is computed in watts as follows:

$$\Psi'_j(S_x, t) = 10^{(\Psi_j^{avg}(S_x) + N(0, \sigma_{ch}))/10} \quad (21)$$

and $\overline{\Psi}_j^{adj}(t)$ is the noise power plus white Gaussian noise (in watts), which can be obtained through substituting $\overline{\Psi}_i^{adj}$ from Eq. (12) in Eq. (3).

Since the *Wireless Channel* module immediately delivers a received message to the nodes in the transmitter's *In-Range Vector*, packet reception duration should be modeled at the *Physical Layer* module. As recent simulators employ object-oriented programming, they can model packet transmission between nodes through objects. For example, a *Message* object in the OMNeT++ simulation framework can be modified to include various data types. Therefore, having a duration field in each packet object, each node's *Physical Layer* can use timers to update its signal list (i.e., **S**). In particular, when a packet arrives at the *Physical Layer*, that signal is added to **S**, and it is removed from **S** when the packet reception duration is finished. This should be noted that this is irrespective to the decision made by the packet reception algorithm.

The proposed architecture can be used for implementing various models in existing simulation tools. However, as mentioned in Section 4, we employed the OMNeT++ simulation framework to develop the simulation tool used in this paper, because this framework only provides the basis required to develop a new simulation tool. Therefore, we could easily implement new modules, without elimination or modifying any existing module.

When the relationship between packet transmission duration and mobility speed allows us to assume that the variation of reception power during a packet reception is negligible, node mobility can be modeled as follows: Whenever a node moves, it can notify the *Wireless Channel* module about its new position. As a position change may affect the signal level between nodes, the *Wireless Channel* module should update the *In-Range Vectors*. The update cost is $O(|\mathbf{V}|^2)$.

The proposed architecture can also be used for evaluating transmission power control protocols. Although wireless transceivers allow transmission power configuration, the transmission power is fixed for at least a packet transmission duration. Therefore, whenever the transmission power of a node changes, the *In-Range Vector* of that node should be updated. The update cost is $O(|\mathbf{V}|)$.

7.2.1. Effect on simulation speed

The aforementioned architecture includes various models with different computational demands. This section aims to discuss about the effects of these models on simulation speed.

- Hardware heterogeneity: At simulation initialization, using a hardware heterogeneity model (cf. Section 3.6) each node computes the deviation of its noise floor and transmission power from the average computed values. Each node also informs the *Wireless Channel* module about its adjusted transmission power value. As these values are fixed for each node throughout a simulation experiment, they do not affect simulation speed. However, it should be noted that the transmission power increment caused by hardware heterogeneity may increase the effect of a node's transmission on other nodes. With respect to interference, increasing the interference range of a node results in higher number of signal arrivals at other nodes, and this increases the number of computations related to the packet reception algorithm. Furthermore, as increasing a node's transmission power may increase the number of neighbors that can receive this node's packet, the number of computations pertaining to packet reception algorithm intensifies. Similarly, since reducing a node's noise floor may increase the chance of packet reception, the computations pertaining to packet reception algorithm increases.
- Radio irregularity: Similar to hardware heterogeneity, the computations regarding radio irregularity are only performed at simulation initialization and they do not have any effect on simulation speed. However, as the increment or decrement of transmission power affect the signal relationship between nodes, radio irregularity may affect the computations pertaining to packet reception algorithm.
- Log-normal shadowing model: The fixed part of this model (i.e., $PL(d_0) + 10\eta \log(d/d_0)$) has been implemented in the *Wireless Channel* module (cf. Eq. (19)), therefore it has no effect on simulation speed. However, as the variable part (i.e., $N(0, \sigma_{ch})$) is implemented within the SINR model (cf. Eqs. (20) and (21)), its overhead depends on the number of signals arriving at each node and the number of packets that can be received by each node.
- Noise floor variations: As this model is implemented within the SINR model (cf. Eq. (20)), its overhead depends on the number of signals arriving at each node and the number of packets that can be received by each node.

7.3. Propagation range optimization

This section addresses simulation speed improvement thorough propagation range confinement. Propagation range considerably influences the simulation speed. Specifically, as long as there are some nodes that their propagation range does not cover the entire network, increasing the propagation range reduces the simulation speed, which is due to the increase in computational and memory management costs. For example, each signal arrival at a node triggers the packet reception algorithm to perform some computations regarding the power of the new signal or the SINR of the signal currently begin received. On the other hand, increasing the propagation range intensifies the number of generated events, which increases the memory management costs. For example, more number of packet copies should be generated and delivered to the nodes. This section, first, studies the existing propagation range confinement methods, then, the effects of propagation range confinement are evaluated in terms of simulation speed and accuracy.

7.3.1. Existing approaches

With respect to the considerable effects of propagation range on simulation scalability (Hamida et al., 2008; Hu and Hou, 2005),

most of the simulators confine the propagation range to improve the simulation speed. In Castalia, a transmitted signal is delivered to a node if the received signal power at the receiver is about 10 dB lower than the noise floor. In GloMoSim, the area is divided into sub-areas, and a message transmitted by a node is only delivered to its neighboring sub-areas. GTNetS defines an interference range for signal propagation. In NS2 CTM, the *WirelessPhy* module delivers a signal to the MAC layer if its received signal power is higher than the carrier-sensing threshold.

Through considering CSMA as the MAC protocol, Ji et al. (2004) have tried to measure the distance beyond which the aggregate reception power is lower than a threshold value and the reception power does not affect the carrier-sensing performance. First, the authors define the *effective node density* (ρ_{eff}), which is defined as the maximum node density that concurrent transmission of the neighboring nodes cannot cause busy carrier sensing. Effective node density is presented as $\rho_{eff} \leq 2/(\sqrt{3}d_{cs}^2)$, where d_{cs} is the distance at which the received signal power is equal to the carrier-sensing threshold. Then, through assuming a disk-shape area with radius d_{radius}, the authors computed the aggregate reception power at the disk center from the nodes outside of a specific distance d_{prop}. Considering the aggregate power should be lower than a specific threshold χ, the following inequality should hold,

$$\frac{2\cdot\pi\cdot\rho_{eff}\cdot\Omega\cdot d_0^{\eta}}{(2-\eta)\cdot PL(d_0)}((d_{radius})^{2-\eta}-(d_{prop})^{2-\eta})<\chi \tag{22}$$

where Ω is the transmission power of the nodes. The above inequality can be used to compute the optimal propagation range d_{prop} as follows:

$$d_{prop}\geq\left((d_{radius})^{2-\eta}-\frac{(2-\eta)\cdot\chi\cdot PL(d_0)}{2\cdot\pi\cdot\rho_{eff}\cdot\Omega\cdot d_0^{\eta}}\right)^{1/2-\eta} \tag{23}$$

Ji et al. have considered $\chi=(\overline{\Psi})^2$, where $\overline{\Psi}$ is the noise floor. They state that this value has been selected based on the empirical experiments with 802.11b networks. However, when we considered this value in low-power wireless simulations, the achieved d_{prop} was always equal to network radius. Unfortunately, the authors have not presented any approach to compute the optimal χ value according to network characteristics. Therefore, we define a new definition of χ in our analyses of Section 7.3.2.

Blough et al. (2009, 2008) proved a theorem on the maximum received signal power from the nodes outside a specific distance. In particular, assuming the log-distance path-loss model, $\eta>2$, identical transmission powers, and constant node density, they proved that the receivable interference at node i (denoted by I_i) from the nodes located at distance $d>d_{intf}$ is

$$I_i\leq\frac{\pi\cdot\rho\cdot\Omega}{(d_{intf})^{\eta-2}}\times\frac{1}{4-5\left(\frac{4}{5}\right)^{\eta/2}} \tag{24}$$

where d_{intf} is the interference range, $d_{intf}\geq 2d_{trans}$, d_{trans} is the transmission range, and ρ is the node density. They showed that if d_{intf} has a constant value, I_i would be significantly higher than the noise floor to deviate the results. Specifically, if d_{intf} can be represented as $f(n)$, which is an arbitrary unbounded increasing function of n, then I_i converges to 0 as $n\to\infty$. Unfortunately, they did not show how to compute the optimal propagation range for a given network setting.

7.3.2. Propagation range versus simulation accuracy and speed

In this section, we analyze the effects of propagation range confinement on the performance evaluation of low-power wireless networks. Instead of presenting the propagation range directly, we show it as $\beta\times d_{TR}$, where β is the coefficient, and d_{TR} is the transitional region size. Accordingly, since the transitional region size is a measurable parameter for a given network setting, we show how increasing the coefficient of the transitional region affects performance evaluations. With respect to the architecture given in Section 7.2, the *In-Range Vector* of a sample node V_i only includes those nodes that are within distance $\beta\times d_{TR}$. This is a straightforward approach to confine the propagation range. In our analyses we also show the propagation range computed through the approach proposed by Ji et al. (2004) (Section 7.3.1). However, we defined $\chi=\overline{\Psi}/\alpha$, and vary the α value to limit the tolerable interference intensity. α is referred to as the *sensitivity denominator*.

Figs. 17, 18 and 19 show our results. While the lower x-axis shows the transitional region coefficient (β), the upper x-axis shows the real propagation distance. Therefore, when the sensitivity denominator is changed, the upper x-axis reflects signal propagation distance. We use two variations of the high-interference broadcast scenario: with CSMA, and without CSMA. Using CSMA, we measure how interference control through carrier sensing affects the results. It is worth noting that simulation speed is in terms of *simulation second/second*, which indicates how fast the simulation proceeds with respect to real time.

Our results show that when the propagation range is at least two-fold higher than the transitional region size, performance evaluations are *almost* accurate. Furthermore, highest accuracy can be achieved when the propagation range is three times larger than the transitional region size. However, although increasing the propagation range from $2d_{TR}$ to $3d_{TR}$ results in up to 10%

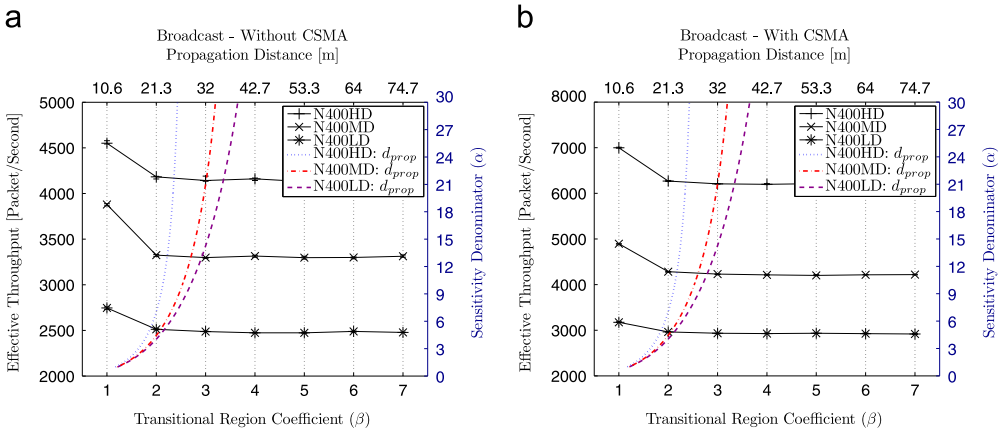

Fig. 17. Effects of propagation range confinement on network throughput. When the propagation range is at least twice the transitional region size, the number of packet receptions can accurately be measured.

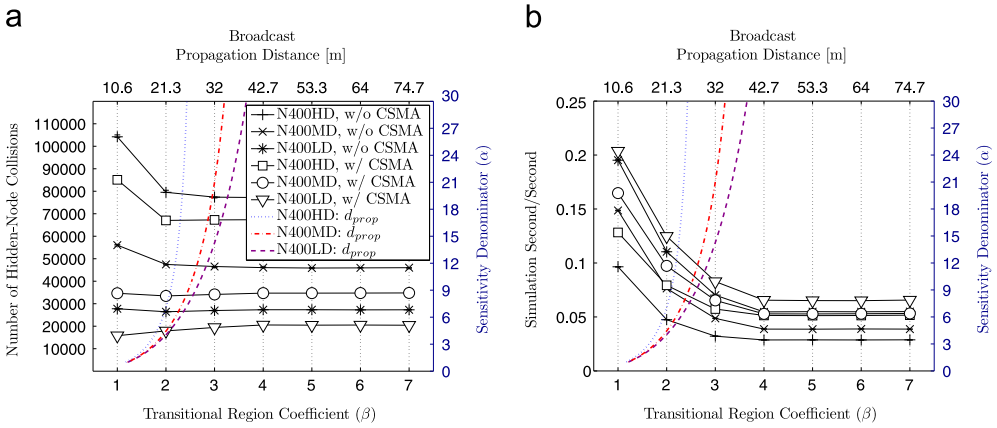

Fig. 18. Effects of propagation range confinement on the number of hidden-node collisions (a), and simulation speed (b).

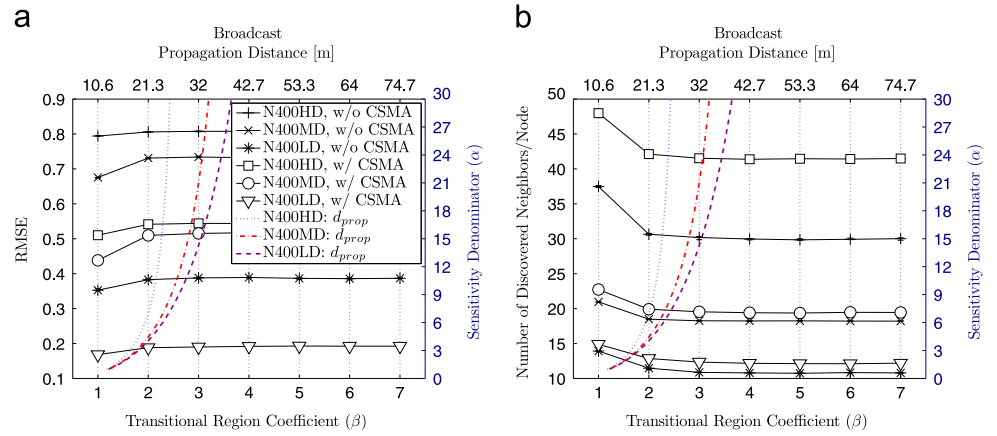

Fig. 19. Effects of propagation range confinement on NDLE performance. (a) Link estimation accuracy (RMSE); (b) average number of discovered neighbors per node.

improvement in evaluation accuracy, this comes at the cost of at least 30% reduction in the simulation speed. As the transitional region can easily be computed for a given network setting, these results suggest that network simulators can easily utilize the transitional region size to confine the propagation range.

With respect to the approach proposed by Ji et al. (2004), we cannot find an optimal α value for different densities. For example, while the minimum α value for high densities is about 20, this value is about 10 for medium and low-density networks. Therefore, as we argued earlier, the major drawback of this approach is to determine the value of χ for a given network setting.

Figure 18(a) shows that for high network densities, when the propagation range increases from d_{TR} to $2d_{TR}$, the number of hidden-node collisions significantly reduces. The question is how increasing the interference range results in lower collisions. The reason can be explained with respect to the packet synchronization concept given in Section 2.1. When the propagation range equals to d_{TR}, a node's sent signal has high chance of synchronization with the nodes in the propagation range. Therefore, the arrival of an interfering signal has higher chance of corrupting an ongoing packet reception. Apparently, lower network density reduces the number of synchronizations per transmission, which in turn causes lower collisions.

8. Conclusion and future directions

In this paper, we presented the state-of-the-art models proposed for low-power wireless communications. We showed the implications of these models on performance evaluation, and we proposed some improvements. With respect to the models presented in this paper, Table 7 compares the features of the most commonly used simulators. This table indicates that none of the existing simulators employs all the essential models. Therefore, many of the performance evaluation results reported in the literature are not valid.

Based on our studies and analyses, we suggest the followings as the future research directions:

(i) According to Table 7, most of the simulators need to be improved from various aspects. However, many of the required changes cannot easily be implemented and may need extensive architectural redesign. On the other hand, since implementing some of these models have negative influence on simulation efficiency, proposing and comparing efficient implementation techniques are required.

(ii) Although most of the characteristics of CC1000 and CC2420 have been investigated, the literature presents less evaluations conducted with transceivers such as CC2500 and CC1120.

(iii) While our results confirm the considerable effects of system variations and radio irregularity on NDLE, CSMA MAC and routing protocols, these characteristics also affect other protocols. In particular, investigations are required to study the influence of the various characteristics of wireless communications on the performance of protocols such as localization, TDMA-based channel access, multipath routing, time synchronization and data aggregation. In addition to clarifying

Table 7
Characteristics of network simulators.

Simulator	Path Loss	Interference	Packet Reception	Propagation Range	Radio Irregularity	Separate Preamble and MPDU Handling	External Interference	Noise Floor/ Transmission Power Heterogeneity
NS2 CTM (NS-2, 2014) (NS2.32 and below)	Log-Normal Shadowing	Capture Threshold	SINR Threshold	Bounded: Constant	No	No	No	No/No
NS2 AIM (NS-2, 2014) (NS2.33 and above)	Log-Normal Shadowing	SINR	SINR Threshold	Unbounded	No	Yes	No	No/No
NS3 (NS-3, 2014)	Log-Normal Shadowing	SINR	BER: BPSK, QPSK, QAM	Unbounded	No	Yes	No	No/No
GloMoSim (GloMoSim, 2014)	Two Ray, Free Space	SINR	BER: BPSK, QPSK	Bounded: Constant	Yes	No	No	No/No
GTNetS (Riley;GTNetS, 2013)	Two Ray, Free Space	Capture Threshold	SINR Threshold	Bounded: Constant	No	No	No	No/No
OMNeT++ Castalia (Castalia, 2011)	Log-Normal Shadowing	SINR	BER: For PSK, FSK	Bounded: Constant	No	No	No	No/No
OMNeT++ MiXiM (Köpke et al.;MiXiM, 2014)	Log-Normal Shadowing	SINR	BER: For OQPSK, GFSK	Bounded: Constant	No	No	No	No/No
TOSSIM (Levis et al., 2003; TOSSIM, 2014)	Log-Normal Shadowing	SINR	Empirical Traces for a Particular Packet Size	Bounded, Unbounded	No	No	Yes	Yes/Yes

the real-world performance of network protocols, these investigations also reveal new design challenges that should be addressed by the research community.

(iv) As our results confirm the considerable effects of propagation range on simulation speed, accurate confinement of propagation range is required to achieve simulation scalability.

References

Ababneh N. Radio irregularity problem in wireless sensor networks: new experimental results. In: IEEE Sarnoff symposium, SARNOFF '09. Princeton, NJ, USA: IEEE; 2009. p. 1–5.

Ahn G-S, Hong SG, Miluzzo E, Campbell AT, Cuomo F. Funneling-MAC: a localized, sink-oriented MAC for boosting fidelity in sensor networks. In: Proceedings of the 4th international conference on embedded networked sensor systems – SenSys '06. Boulder, Colorado, USA: ACM Press; 2006. p. 293.

Al-Bado M, Sengul C, Merz R. What details are needed for wireless simulations? – A study of a site-specific indoor wireless model. In: The 31st annual IEEE international conference on computer communications (INFOCOM'12). Orlando, FL, USA: IEEE; 2012. p. 289–97.

Biaz S. Realistic radio range irregularity model and its impact on localization for wireless sensor networks. In: Proceedings of international conference on wireless communications, networking and mobile computing (WiCOM), vol. 2. IEEE; 2005. p. 669–73.

Blough DM, Canali C, Resta G, Santi P. On the impact of far-away interference on evaluations of wireless multihop networks. Technical Report, IIT-CNR, Tenerife, Canary Islands, Spain; 2008.

Blough DM, Canali C, Resta G, Santi P. On the impact of far-away interference on evaluations of wireless multihop networks. In: Proceedings of the 12th ACM international conference on modeling, analysis and simulation of wireless and mobile systems – MSWiM '09. Tenerife, Canary Islands, Spain: ACM Press; 2009. p. 90.

Cardieri P. Modeling interference in wireless ad hoc networks. IEEE Commun Surv Tutor 2010;12:551–72.

Castalia. A simulator for wireless sensor networks, ⟨http://castalia.research.nicta.com.au/⟩; 2011.

CC1120, High performance RF transceiver for narrowband systems, ⟨www.ti.com/product/cc1120⟩; 2014.

CC2500, Single chip low cost low power RF transceiver, ⟨www.ti.com/product/cc2500⟩; 2014.

Cerpa A, Wong JL, Potkonjak M, Estrin D. Temporal properties of low power wireless links. In: Proceedings of the 6th ACM international symposium on Mobile ad hoc networking and computing – MobiHoc '05, January. Urbana-Champaign, IL, USA: ACM Press; 2005. p. 414.

Chen Y, Terzis A. On the implications of the log-normal path loss model. In: Proceedings of the 9th ACM conference on embedded networked sensor systems – SenSys '11. Seattle, Washington, USA: ACM Press; 2011. p. 26.

Chen Q, Jiang D, Taliwal V, Delgrossi L. IEEE 802.11 based vehicular communication simulation design for NS-2. In: Proceedings of the 3rd international workshop on vehicular ad hoc networks – VANET '06. Los Angeles, CA, USA: ACM Press; 2006. p. 50.

Chen Q, Schmidt-Eisenlohr F, Jiang D, Torrent-Moreno M, Delgrossi L, Hartenstein H. Overhaul of IEEE 802.11 modeling and simulation in ns-2. In: Proceedings of the 10th ACM symposium on modeling, analysis, and simulation of wireless and mobile systems – MSWiM '07. Chania, Crete Island, Greece: ACM Press; 2007. p. 159.

Chipcon CC1000, Single chip very low power RF transceiver, ⟨www.ti.com/lit/ds/symlink/cc1000.pdf⟩; 2014.

Chipcon CC2420, 2.4 GHz IEEE 802.15.4/ZigBee-ready RF Transceiver, ⟨http://www.ti.com/lit/gpn/cc2420⟩; 2014.

Couto D, Aguayo D, Bicket J, Morris R. A high-throughput path metric for multi-hop wireless routing. Wirel Netw 2005;11:419–34.

Dezfouli B, Radi M, Nematbakhsh MA, Razak SA. A medium access control protocol with adaptive parent selection mechanism for large-scale sensor networks. In: International conference on advanced information networking and applications – WINA "11. Biopolis, Singapore: IEEE; 2011. p. 402–8.

Dezfouli B, Radi M, Razak SA, Whitehouse K, Bakar KA, Hwee-Pink T. Improving broadcast reliability for neighbor discovery, link estimation and collection tree construction in wireless sensor networks. Comput Netw 2014;62:101–21, http://dx.doi.org/10.1016/j.comnet.2014.01.002.

Evans D, Krasinski R, Batra A, Dawkins M, Hosur S, Wang D. IEEE P802.15 wireless personal area networks: coexistence assurance document. Technical Report, IEEE; 2012.

Firner B, Xu C, Howard R, Zhang Y. Multiple receiver strategies for minimizing packet loss in dense sensor networks. In: Proceedings of the 11th ACM international symposium on Mobile ad hoc networking and computing – MobiHoc '10. Chicago, Illinois, USA: ACM Press; 2010. p. 211.

Ganesan D, Krishnamachari B, Woo A, Culler D, Estrin D, Wicker S. Complex behavior at scale: an experimental study of low-power wireless sensor networks. Technical Report 02-0013, UCLA Computer Science Division; 2002.

Gezer C, Buratti C, Verdone R. Capture effect in IEEE 802.15.4 networks: modelling and experimentation. In: IEEE 5th international symposium on wireless pervasive computing, ISWPC'10, ii. Mondena, Italy: IEEE; 2010. p. 204–9.

Girod L, Ramanathan N, Elson J, Stathopoulos T, Lukac M, Estrin D. Emstar. ACM Trans Sensor Netw 2007;3:13.

GloMoSim. Global mobile information systems simulation library, ⟨http://pcl.cs.ucla.edu/projects/glomosim/⟩; 2014.

Gnawali O, Fonseca R, Jamieson K, Kazandjieva M, Moss D, Levis P. CTP: an efficient, robust, and reliable collection tree protocol for wireless sensor networks. ACM Trans Sensor Netw 2013;10:1–49.

GTNetS, The Georgia tech network simulator, ⟨www.ece.gatech.edu/research/labs/MANIACS/GTNetS⟩; 2013.

Gupta P, Kumar PR. The capacity of wireless networks. IEEE Trans Inf Theory 2000;46:388–404.

Halkes G, Langendoen K. Experimental evaluation of simulation abstractions for wireless sensor network MAC protocols. EURASIP J Wireless Commun Netw 2010:1–11.

Hamida EB, Chelius G, Gorce J-M. Scalable versus accurate physical layer modeling in wireless network simulations. In: Proceedings of the 22nd conference on principles of advanced and distributed simulation (PADS '08). Washington, DC, USA: IEEE; 2008. p. 127–34.

He T, Huang C, Blum BM, Stankovic JA, Abdelzaher T. Range-free localization schemes for large scale sensor networks. In: Proceedings of the 9th annual international conference on Mobile computing and networking – MobiCom '03. San Diego, CA, USA: ACM Press; 2003. p. 81.

Hu C, Hou JC. A reactive channel model for expediting wireless network simulation. SIGMETRICS Perform Eval Rev 2005;33:410.

IEEE Computer Society, IEEE 802.15: wireless personal area networks (PANs). Part 15.2: coexistence of wireless personal area networks with other wireless devices operating in unlicensed frequency band; 2003.

IEEE Computer Society, IEEE 802.15: wireless personal area networks (PANs). part 15.4: low-rate wireless personal area networks (LR-WPANs); 2012.

Iyer A, Rosenberg C, Karnik A. What is the right model for wireless channel interference? IEEE Trans Wirel Commun 2009;8:2662–71.

Ji Z, Zhou J, Takai M, Bagrodia R. Scalable simulation of large-scale wireless networks with bounded inaccuracies. In: Proceedings of the 7th ACM international symposium on Modeling, analysis and simulation of wireless and mobile systems – MSWiM '04. Venice, Italy: ACM Press; 2004. p. 62.

Jung ES, Vaidya NH. A power control MAC protocol for ad hoc networks. In: Proceedings of the 8th annual international conference on Mobile computing and networking – MobiCom '02, vol. 11. Atlanta, Georgia, USA: ACM Press; 2002. p. 36.

Jurdak R, Baldi P, Videira Lopes C. Adaptive low power listening for wireless sensor networks. IEEE Trans Mob Comput 2007;6:988–1004.

Karl H, Willig A. Protocols and architectures for wireless sensor networks. Chichester, UK: John Wiley & Sons Ltd; 2005.

Kim JH, Lee JK. Capture effects of wireless CSMA/CA protocols in Rayleigh and shadow fading channels. IEEE Trans Veh Technol 1999;48:1277–86.

Kochut A, Vasan A, Shankar A, Agrawala A. Sniffing out the correct physical layer capture model in 802.11b. In: Proceedings of the 12th IEEE international conference on network protocols – ICNP '04. IEEE; 2004: p. 252–61.

Köpke A, Swigulski M, Wessel K. Simulating wireless and mobile networks in OMNeT++ the MiXiM vision. In: Proceedings of the 1st international conference on simulation tools and techniques for communications, networks and systems & workshops, Simutools '08, Brussels, Belgium. p. 71.

Kotz D, Newport C, Gray RS, Liu J, Yuan Y, Elliott C. Experimental evaluation of wireless simulation assumptions. In: Proceedings of the 7th ACM international symposium on modeling, analysis and simulation of wireless and mobile systems – MSWiM '04. Venice, Italy: ACM Press; 2004. p. 78–82.

Kuntz A, Schmidt-Eisenlohr F. Introducing probabilistic radio propagation models in OMNeT++ mobility framework and cross validation check with ns-2. In: Proceedings of the 1st international conference on simulation tools and techniques for communications, networks and systems & workshops, Simutools '08. Marseille, France. p. 72.

Langendoen K. Medium access control in wireless sensor network. In: Medium access control in wireless networks, vol. II. Nova Science Publishers, Inc.; 2008. p. 535–60.

Lee J, Kim W, Lee S-J, Jo D, Ryu J, Kwon T, et al. An experimental study on the capture effect in 802.11a networks. In: Proceedings of the second ACM international workshop on Wireless network testbeds, experimental evaluation and characterization – WinTECH '07. Montreal, Quebec, Canada: ACM Press; 2007. p. 19.

Lee H, Cerpa A, Levis P. Improving wireless simulation through noise modeling. In: Proceedings of the 6th international conference on Information processing in sensor networks – IPSN '07. Cambridge, MA, USA: ACM Press; 2007. p. 21.

Lee J, Ryu J, Lee S-J, Kwon TT. Improved modeling of IEEE 802.11a PHY through fine-grained measurements. Comput Netw 2010a;54:641–57.

Lee PWQ, Seah WKG, Tan H-P, Yao Z. Wireless sensing without sensors – an experimental study of motion/intrusion detection using RF irregularity. Meas Sci Technol 2010b;21:124007.

Levis P, Lee N, Welsh M, Culler D. TOSSIM: accurate and scalable simulation of entire TinyOS applications. In: Proceedings of the 1st international conference on Embedded networked sensor systems (SenSys'03). Los Angeles, California, USA: ACM; 2003. p. 126–37.

Levis P, Madden S, Polastre J, Szewczyk R, Whitehouse K, Woo A, et al. Tinyos: an operating system for sensor networks. In: Ambient intelligence, vol. 35. Springer Verlag; 2005. p. 115–48 ⟨http://link.springer.com/chapter/10.1007%2F3-540-27139-2_7⟩.

Li X-Y. Multicast capacity of wireless ad hoc networks. IEEE/ACM Trans Netw 2009;17:950–61.

Li J, Blake C, De Couto DS, Lee HI, Morris R. Capacity of Ad Hoc wireless networks. In: Proceedings of the 7th annual international conference on Mobile computing and networking (MobiCom '01), 1. Rome, Italy: ACM Press; 2001. p. 61–9.

Lu J, Whitehouse K. Flash flooding: exploiting the capture effect for rapid flooding in wireless sensor networks. In: The 28th conference on computer communications (INFOCOM '09). Rio de Janeiro, Brazil: IEEE; 2009. p. 2491–99.

Maheshwari R, Jain S, Das SR. On estimating joint interference for concurrent packet transmissions in low power wireless networks. In: Proceedings of the third ACM international workshop on wireless network testbeds, experimental evaluation and characterization – WiNTECH '08. San Francisco, California, USA: ACM Press; 2008. p. 89.

Maheshwari R, Jain S, Das SR. A measurement study of interference modeling and scheduling in low-power wireless networks. In: Proceedings of the 6th ACM conference on Embedded network sensor systems – SenSys '08. Raleigh, NC, USA: ACM Press; 2008. p. 141.

Martnez-Sala A, Molina-Garca-Pardo JE. An accurate radio channel model for wireless sensor networks simulation. J Commun Netw 2005;7:1–7.

Mica2, Wireless measurement system, ⟨www.xbow.com⟩; 2014.

MicaZ, Wireless measurement system, ⟨www.xbow.com⟩; 2014.

MiXiM T. Simulating wireless and mobile networks in OMNeT++, ⟨http://mixim.sourceforge.net/⟩; 2014.

Molina-Garcia-Pardo J, Martinez-Sala A, Bueno-Delgado M, Egea-Lopez E, Juan-Llacer L, Garcia-Haro J. Channel model at 868 MHz for wireless sensor networks in outdoor scenarios. In: Proceedings of the international workshop on wireless ad-hoc networks (IWWAN 2005). p. 2–5.

Muetze T, Stuedi P, Kuhn F, Alonso G. Understanding radio irregularity in wireless networks. In: 5th annual IEEE communications society conference on sensor, mesh and Ad Hoc communications and networks, SECON '08. San Francisco, CA, USA: IEEE; 2008. p. 82–90.

Nikookar H, Hashemi H. Statistical modeling of signal amplitude fading of indoor radio propagation channels. In: Proceedings of 2nd IEEE international conference on universal personal communications, vol. 1. Ottawa, Ontario, Canada: IEEE; 1993. p. 84–8.

NS-2, Network simulator, ⟨http://www.isi.edu/nsnam/ns/⟩; 2014.

NS-3, Network simulator, ⟨http://www.nsnam.org/⟩; 2014.

OMNeT++, The OMNeT++ network simulation framework, ⟨http://www.omnetpp.org⟩; 2014.

Papanastasiou S, Mittag J, Strom EG, Hartenstein H. Bridging the gap between physical layer emulation and network simulation. In: IEEE wireless communication and networking conference (WCNC), vol. 9. Sydney, Australia: IEEE; 2010. p. 1–6.

Polastre J, Hill J, Culler D. Versatile low power media access for wireless sensor networks. In: Proceedings of the 2nd international conference on embedded networked sensor systems (SenSys '04). Baltimore, MD, USA: ACM Press; 2004. p. 95.

Radi M, Dezfouli B, Bakar KA, Razak SA, Nematbakhsh MA. Interference-aware multipath routing protocol for QoS improvement in event-driven wireless sensor networks. Tsinghua Sci Technol 2011;16:475–90.

Radi M, Dezfouli B, Bakar KA, Lee M. Multipath routing in wireless sensor networks: survey and research challenges. Sensors (Basel, Switzerland) 2012;12:650–85.

Radi M, Dezfouli B, Bakar KA, Razak SA, Lee M. Network initialization in low-power wireless networks: a comprehensive study. Comput J. 2013, http://dx.doi.org/10.1093/comjnl/bxt074.

Rappaport TS. Wireless communications: principles and practice. 2nd Edition Upper Saddle River, NJ, USA: Prentice Hall; 2002.

Reijers N, Halkes G, Langendoen K. Link layer measurements in sensor networks. In: IEEE international conference on mobile ad-hoc and sensor systems (MASS '04). IEEE; 2004: p. 224–34.

Reis C, Mahajan R, Rodrig M, Wetherall D, Zahorjan J. Measurement-based models of delivery and interference in static wireless networks. ACM SIGCOMM Comput Commun Rev 2006;36:51.

Riley G. 2013. The Georgia Tech network simulator. In: Proceedings of the ACM SIGCOMM workshop on models, methods and tools for reproducible network research (MoMeTools '03), August. Karlsruhe, Germany, p. 5–12.

Rusak T, Levis PA. Investigating a physically-based signal power model for robust low power wireless link simulation. In: Proceedings of the 11th international symposium on modeling, analysis and simulation of wireless and mobile systems – MSWiM '08. Vancouver, British Columbia, Canada: ACM Press; 2008. p. 37.

Ryu J, Lee J, Lee S-J, Kwon T. Revamping the IEEE 802.11a PHY simulation models. In: Proceedings of the 11th international symposium on modeling, analysis and simulation of wireless and mobile Systems – MSWIM '08. Vancouver, British Columbia, Canada: ACM Press; 2008. p. 28.

Schmidt-eisenlohr F, Letamendia-murua J, Torrent-moreno M, Hartenstein H. Bug Fixes on the IEEE 802.11 DCF module of the network simulator ns-2.28. Technical Report, Department of Computer Science, University of Karlsruhe; 2006.

Seada K, Zuniga M, Helmy A, Krishnamachari B. Energy-efficient forwarding strategies for geographic routing in lossy wireless sensor networks. In: Proceedings of the 2nd international conference on embedded networked sensor systems – SenSys '04. Baltimore, MD, USA: ACM Press; 2004. p. 108.

Seidel S, Rappaport T. 914 MHz path loss prediction models for indoor wireless communications in multifloored buildings. IEEE Trans Antennas Propag 1992;40:207–17.

Shin SY, Choi S, Park HS, Kwon WH. Packet error rate analysis of IEEE 802.15.4 under IEEE 802.11b interference. In: Wired/wireless internet communications. Berlin Heidelberg: Springer; 2005. p. 279–88.

Sohrabi K, Manriquez B, Pottie G. Near ground wideband channel measurement in 800–1000 MHz. In: IEEE 49th vehicular technology conference, vol. 1. Houston, TX, USA: IEEE; 1999. p. 571–4.

Son D, Krishnamachari B, Heidemann J. Experimental study of concurrent transmission in wireless sensor networks. In: Proceedings of the 4th international conference on embedded networked sensor systems – SenSys '06. Boulder, Colorado, USA: ACM Press; 2006. p. 237.

Son D, Krishnamachari B, Heidemann J. Evaluating the importance of concurrent packet communication in wireless networks. Technical Report April, USC/ISI Technical Report ISI-TR-639; 2007.

Srinivasan K, Dutta P, Tavakoli A, Levis P. An empirical study of low-power wireless. ACM Trans Sensor Netw 2010;6:1–49.

Stankovic J, Abdelzaber T. RID: radio interference detection in wireless sensor networks. In: Proceedings IEEE 24th annual joint conference of the IEEE computer and communications societies, INFOCOM '05, vol. 2. IEEE; 2005. p. 891–901.

TelosB, TelosB mote platform, ⟨www.xbow.com⟩; 2014.

TinyOS, Operating system for low-power wireless devices, ⟨http://www.tinyos.net/⟩; 2013.

TOSSIM, TinyOS simulator, ⟨http://docs.tinyos.net/tinywiki/index.php/TOSSIM⟩; 2014.

TR1000, 916.50 MHz hybrid transceiver, ⟨http://www.rfm.com/products/data/tr1000.pdf⟩; 2014.

Varshney M, Bagrodia R. Detailed models for sensor network simulations and their impact on network performance. In: Proceedings of the 7th ACM international symposium on Modeling, analysis and simulation of wireless and mobile systems – MSWiM '04. Venice, Italy: ACM Press; 2004. p. 70.

Wang W, Li X-Y, Frieder O, Wang Y, Song W-Z. Efficient interference-aware TDMA link scheduling for static wireless networks. In: Proceedings of the 12th annual international conference on Mobile computing and networking – MobiCom '06. Los Angeles, CA, USA: ACM Press; 2006. p. 262.

Whitehouse K, Woo A, Jiang F, Polastre J, Culler D. Exploiting the capture effect for collision detection and recovery. In: The second IEEE workshop on embedded networked sensors, 2005. EmNetS-II. Sydney, Australia: IEEE; 2005. p. 45–52.

Woo S, Kim H. Estimating link reliability in wireless networks: an empirical study and interference modeling. In: Proceedings IEEE INFOCOM'10. IEEE; 2010. p. 1–5.

Woo A, Tong T, Culler D. Taming the underlying challenges of reliable multihop routing in sensor networks. In: Proceedings of the 1st international conference on Embedded networked sensor systems – SenSys '03. Los Angeles, California, USA: ACM Press; 2003. p. 14–27.

Xu H, Garcia-Luna-Aceves JJ, Hamid RS. Exploiting the capture effect opportunistically in MANETs. In: Proceedings of the military communication conference (MILCOM'10). San Jose, CA, USA: IEEE; 2010. p. 1490–5.

Ye W, Silva F, Heidemann J. Ultra-low duty cycle MAC with scheduled channel polling. In: Proceedings of the 4th international conference on Embedded networked sensor systems (SenSys '06). Boulder, Colorado, USA: ACM Press; 2006. p. 321.

Yun J-H, Seo S-W. Novel collision detection scheme and its applications for IEEE 802.11 wireless LANs. Comput Commun 2007;30:1350–66.

Zamalloa M, Krishnamachari B. Analyzing the transitional region in low power wireless links. In: Proceeding of the first annual IEEE communications society conference on sensor and ad hoc communications and networks – SECON '04. IEEE; 2004. p. 517–26.

Zamalloa MZ, Krishnamachari B. An analysis of unreliability and asymmetry in low-power wireless links. ACM Trans Sensor Netw 2007;3:63–81.

Zhang LQ, Wang F, Han MK, Mahajan R. A general model of wireless interference. In: Proceedings of the 13th annual ACM international conference on Mobile computing and networking - MobiCom '07. Qubec, Canada: ACM Press; 2007. p. 171.

Zhao J, Govindan R. Understanding packet delivery performance in dense wireless sensor networks. In: Proceedings of the 1st international conference on embedded networked sensor systems, SenSys '03. Los Angeles, California, USA: ACM; 2003. p. 1–13.

Zhou G, He T, Krishnamurthy S, Stankovic Ja. Models and solutions for radio irregularity in wireless sensor networks. ACM Trans Sensor Netw 2006;2:221–62.